The role of climate and tectonics in aggradation and incision of the Indus River in the Ladakh Himalaya during the late Quaternary

Anil Kumar and Pradeep Srivastava*
Wadia Institute of Himalayan Geology, 33 GMS Road, Dehradun, India

Abstract

The geomorphic evolution of the upper Indus River that traverses across the southwest (SW) edge of Tibet, and the Ladakh and Zanskar ranges, was examined along a ~350-km-long stretch of its reaches. Based on the longitudinal river profile, stream length gradient index, and river/strath terraces, this stretch of the river is divided into four segments. Valley fill river terraces are ubiquitous, and strath terraces occur in the lower reaches where the Indus River cuts through deformed Indus Molasse. Optically stimulated luminescence ages of river/strath terraces suggest that valley aggradation occurred in three pulses, at ~52, ~28, and ~16 ka, and that these broadly coincide with periods of stronger SW Indian summer monsoon. Reconstructed longitudinal river profiles using strath terraces provide an upper limit on the bedrock and provide incision rates ranging from 1.0 ± 0.3 to 2.2 ± 0.9 mm/a. These results suggested that rapid uplift of the western syntaxes aided by uplift along the local faults led to the formation of strath terraces and increased fluvial incision rates along this stretch of the river.

Keywords: Indus River; NW Ladakh Himalaya; Aggradation-incision; Luminescence dating

INTRODUCTION

Sediment aggradation and incision along Himalayan rivers are influenced by precipitation changes and tectonics (Goodbred, 2003; Bookhagen et al., 2005; Srivastava and Misra, 2008; Srivastava et al., 2008; Ray and Srivastava, 2010; Scherler et al., 2015). Understanding of such riverine processes together with their spatial and temporal changes is central to the understanding of landscape evolution in the Himalaya.

At the valley scale, river aggradation and incision of valley fill sediments have been linked to climate (Pratt-Sitaula et al., 2004; Ray and Srivastava, 2010; Scherler et al., 2015). Incision into the bedrock along with the formation of strath terraces has been linked to rock uplift by tectonic movements (Pazzaglia et al., 1998; Hancock and Anderson, 2002; Dortch et al., 2011a; Srivastava et al., 2013). Studies along rivers draining the southern front of the Himalaya—namely, the Sutlej, Yamuna, Bhagirathi, Alaknanda, and Gandaki, which receive waters from the southwest (SW) Indian summer monsoon (ISM)—have provided an understanding of aggradation and incision cycles and their relationship to climate and tectonics (Lavé and Avouac, 2000; Thiede et al., 2004; Bookhagen et al.,

2005; Juyal et al., 2010; Ray and Srivastava, 2010; Devrani and Singh, 2014; Morell et al., 2015; Sharma et al., 2016a). However, little attention has been given to the rivers that drain the more arid regions of the northwest (NW) Himalaya, which besides the summer monsoon also receive waters from the midlatitude westerlies. These rivers, which include the Indus and its tributaries, are influenced by the tectonic movements associated with the Indus-Tsangpo Suture Zone (ITSZ), the western syntaxes, and the Karakoram Fault (Burbank et al., 1996; Leland et al., 1998; Jamieson et al., 2004; Pant et al., 2005; Phartiyal et al., 2005; Dortch et al., 2011a; Blöthe et al., 2014; Sinclair et al., 2017). The Indus River originates in Tibet, flows through Ladakh, and crosses the western syntaxes and forms a megafan on the plains of Pakistan before reaching the Arabian Sea. Sediments deposited by the river provide useful information on the climate and tectonic regimes through time.

Studies in the upper reaches of the Indus River system have so far dealt with the following: (1) chronology of past glaciations (Derbyshire and Owen, 1997; Owen and Benn, 2005; Owen et al., 2006a; Dortch et al., 2013; Sharma et al., 2016b; Orr et al., 2017); (2) catchment-scale erosion rates (Dortch et al., 2011b; Clift and Giosan, 2014; Munack et al., 2014); (3) neotectonic deformation (Sinclair et al., 2017); (4) phases of aggradation and incision along segments of the

*Corresponding author at: Wadia Institute of Himalayan Geology, 33 GMS Road, Dehradun, India. E-mail: pradeep@wihg.res.in (P. Srivastava).

river and their relationship to climate (Dortch et al., 2011a; Sant et al., 2011a, 2011b; Blöthe et al., 2014); (5) paleolake records (Phartiyal and Sharma, 2009; Sangode et al., 2011, 2013; Sant et al., 2011b); and (6) paraglaciation (Owen et al., 1997, 2001; Pant et al., 2005; Saha et al., 2016; Sharma et al., 2016b). These studies, however, do not provide a synoptic view of the evolution of the upper Indus River and its relation to climate and tectonics.

In the upper reaches of the Indus River, two terrace types exist: (1) valley fill river terraces that rise from the riverbed and preserve sedimentary records of valley aggradation followed by incision; and (2) strath terraces characterized by a fluvially incised bedrock overlain by a thin alluvial sediment cover. Chronology of both the types of terraces enables computation of climate-induced aggradation and bedrock incision rates (Bull, 1990; Pazzaglia et al., 1998; Hancock and Anderson, 2002; Starkel, 2003; Ray and Srivastava, 2010).

Geodetic surveys between Leh and the Karakoram during 1998 and 2008 show statistically insignificant horizontal velocities (0.4 ± 1 mm/a), and this makes it difficult to quantify internal deformation within the ITSZ (Jade et al., 2011). Contrastingly, a recent study on the tectonic geomorphology of the river around Leh indicates a slip of 21 cm/ka during the past ~45 ka. This slip is on the Stok Thrust between Indus Molasse and the Ladakh Batholith (Sinclair et al., 2017).

The present study builds on the work of Sinclair et al. (2017) and provides an optically stimulated luminescence (OSL) chronology for valley fill and strath terraces at 18 locations between the villages of Nyoma (34°37.96′N, 76°27.40′E) and Dah (33°9.37′N, 78°44.12′E). OSL ages combined with geomorphic and sedimentologic data help define the timing and duration of aggradation and bedrock incision and enable the development of a model for the formation of river and strath terraces.

CLIMATE AND GEOLOGY

The study area is located in the rain shadow of the Greater Himalaya and is a cold desert of the Köppen's *BWk* type (Fig. 1). Summers (May to September) are short with mean temperatures of 12.4°C, and winters (October to March) have mean temperatures of −1.4°C (Demske et al., 2009). Annual precipitation in Leh is ~100 mm and occurs mostly as snowfall (Lang and Barros, 2004).The region experiences two climatic systems, the SW ISM and midlatitude westerlies. The ISM advects moisture from the Arabian Sea and the Bay of Bengal, brings rainfall to the Himalaya during the summer, and provides ~50% of the hydrologic budget for the Indus River (Bookhagen et al., 2005; Anders et al., 2006; Hobley et al., 2012). The midlatitude westerlies provide snowfall and contribute the remaining ~50% to the hydrologic budget (Bookhagen and Burbank, 2010).

The river crosses the two principal geologic units of the ITSZ: (1) the Indus Molasse comprising basal shallow marine Zanskar platform sediments (the Tar group) followed by the terrestrial sediments of the Indus group (Thakur and Misra, 1984; Sinclair and Jaffey, 2001; Wu et al., 2007;

Henderson et al., 2010, 2011; Singh et al., 2015); and (2) the granitic Ladakh Batholith (Fig. 1).

The rocks of the Tar and Indus groups form part of the Zanskar ranges and are separated by a high-angle, north-verging back thrust, known as the Choksti Thrust (Thakur, 1983; Searle, 1986; Searle et al., 1990; Sinclair and Jaffey, 2001). In addition, the Indus rocks are internally deformed by a back thrust called the Stok Thrust. The entire package of Indus Molasse is thrusted over the Ladakh Batholith along the north-verging Upshi-Bazgo Thrust (Fig. 1B; Brookfield and Andrews-Speed, 1984; Searle et al., 1990; Sinclair et al., 2017).

METHODOLOGY

A Shuttle Radar Topography Mission (SRTM) digital elevation model (DEM) with a resolution of 3 arc seconds, Survey of India topographic sheets (1:50,000), and field survey were used: (1) to delineate river patterns; (2) to identify terrace types; (3) to construct cross-valley and longitudinal river profile; and (4) for stream length (SL) gradient index analysis.

Morphostratigraphy

Morphostratigraphy of the sections used terrace elevation above the contemporary river level. The active floodplain was named T-0, and the terraces at successively higher elevation were named T-1 (youngest) and T-2 (older). The height of terraces above the contemporary river level (arl) was measured using a total station with a vertical resolution of 2–3 mm. The survey was carried out during August, and therefore, elevations are with respect to the flood stage. Bedrock incision rate based on strath terraces was determined by dividing the height of the terrace by its age. An uncertainty of ± 5% was assumed owing to lateral geomorphic variability of the strath surfaces. Errors in the age and strath height were propagated in the computation of incision rate.

The terrace sediments were described using gravel sizes, roundness, sorting, imbrication, lithology, and matrix percentage. Using these, various lithofacies were identified and vertical graphic sedimentary logs were prepared. Further, genetically related sediment units were classified as lithofacies associations (e.g., facies formed as result of channel processes were considered as genetically related). Clast composition and textural data were determined using a 1×1 m grid that was placed on the exposed face of the sections using Howard (1993).

Chronology

The chronology was based on OSL. Use of radiocarbon dating in the study area has been challenging because of the paucity of datable material and contamination by older carbon supplied from the limestone terrain (Juyal et al., 2009; Phartiyal et al., 2009).

OSL dating is based on the zeroing of the stored luminescence in sediment grains by daylight exposure during
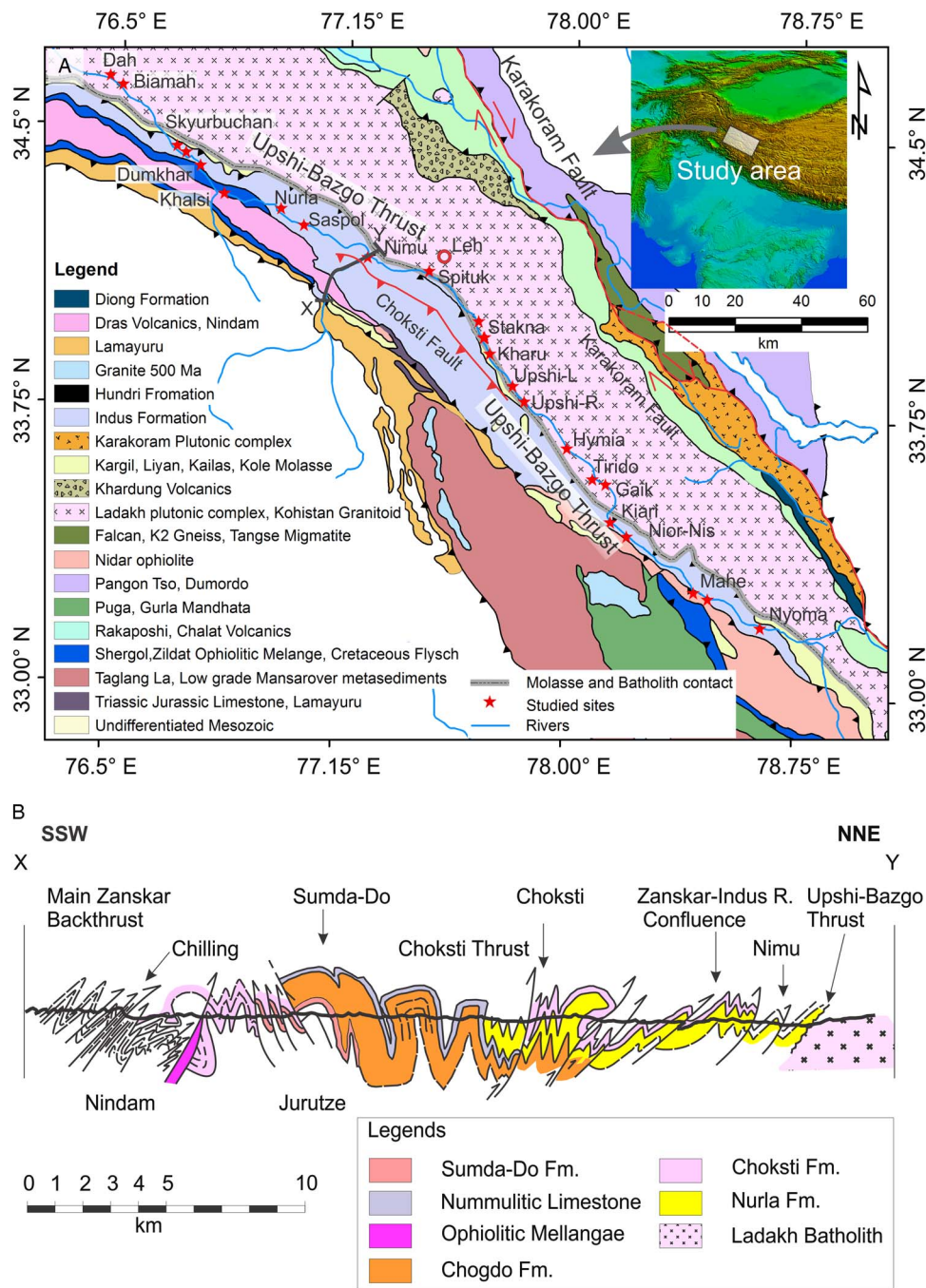
Figure 1. (color online) (A) Geology of the study area, Indus River, and study locations. (B) Geologic cross section along X-Y showing deformation in molasse and presence of north-verging Zanskar Thrust, Choksti Thrust, and Upshi-Bazgo Thrust (after Searle et al., 1990).

erosion, transport, and deposition. Reaccumulation of luminescence is initiated on burial because of irradiation arising from the decay of naturally occurring radionuclides. The luminescence accumulation continues unabated until excavation, and this luminescence carries the information on the age. Conversion of luminescence intensity to radiation dose units is done using OSL measurements and the annual radiation dose. The dating protocol thus includes the following: (1) estimation of the equivalent laboratory beta dose (D_E), which is the laboratory beta dose that induces the

luminescence intensity equal to that which the sediment has received naturally; and (2) computation of annual dose rate (D_T) determined by measuring the elemental concentration of natural U, Th, and K radionuclides and cosmic dose. Samples for OSL dating were collected using stainless-steel tubes and processed using the standard laboratory protocols (Aitken, 1998). Single aliquot regeneration (SAR) method of Murray and Wintle (2000) was used to determine D_E values. Double SAR method was used in seven samples where the feldspar contamination could not be removed by chemical

treatment (see Supplementary Data 1 for SAR and double SAR protocols; Jain et al., 2005).

A critical issue in the reliability of OSL ages is the completeness of zeroing of luminescence prior to burial. This depends on the amount of daylight exposure that was available to mineral grains in the sediment. Turbulence and turbidity of the transporting medium attenuates the intensity and modifies the spectrum daylight. Such conditions lead to heterogeneous zeroing at the grain level and to a wide distribution of D_E values. Based on the existing dating methods and protocols, a mean age model was used for samples with normally distributed D_E values (Galbraith et al., 1999).

The samples were considered well bleached if (1) the luminescence intensity and D_E values for all the measured aliquots were poorly correlated (see Colls et al., 2001) and (2) the ratio of standard deviation and mean of D_E values (the coefficient of variation S_n) was greater than 0.1. Use of criterion 1 indicated that all 33 samples were well bleached, and the use of criterion 2 suggested that 21 samples were well bleached (Clarke, 1996; Srivastava et al., 2006; see Supplementary Data 1 for details). Thus, overall, the mean age model was considered to be appropriate. The D_T was computed by measuring the concentration of U, Th, and K in samples using X-ray fluorescence. Water content was assumed to be $10 \pm 5\%$ by weight, and the cosmic dose was determined using Prescott and Hutton (1994). More details on the methodology and dating protocols are presented in Supplementary Data 1.

River parameters

The SL gradient index and steepness index (K_s) helped delineate tectonic perturbations in the river catchment (Kirby et al., 2003; Morell et al., 2015). SL index was computed using the equation of Hack (1973):

$$SL = \frac{H_1 - H_2}{\ln L_2 - \ln L_1}, \qquad \text{(Eq. 1)}$$

where H_1 and H_2 were the elevation from mean sea level for the points at distances L_1 and L_2 from the source. The K_s index provides the spatially averaged uplift rate (Whipple and Tucker, 1999), but it ignores aspects such as: (1) nonlinearity in incision (Whipple et al., 2000); (2) channel morphology (Lavé and Avouac, 2000, 2001); and (3) riverbed morphology (Hancock and Anderson, 2002; Whipple and Tucker, 2002). However, given that the SL index is related to flow resistance and erodibility contrast at a particular reach of the channel, it depends on lithological changes and tectonics. We used it as a first-order tool to elucidate possible tectonic controls. To compute the SL index, longitudinal river profile was prepared by changing the projection of SRTM DEM from WGS 84 to Lambert conformal conic (to transform the units from degrees to meters). The Environmental System Research Institute's ArcGIS 9.3 software was used for corrections and data processing. Hydrologic tools of ArcGIS and standard protocols to generate a stream from DEM were utilized. Small channels with pixel values less than the trunk channel were deleted, and the fragments were merged to form a single linear stream. The length of the trunk channel was then divided into small segments, each separated by the SRTM DEM pixel size of 90 m. These line features were then converted into points and were added with field x, y (latitude, longitude). The z values (raster values) were extracted from the DEM in the attribute table using the "extract values to the points" tool. The attribute table was exported in text format and used to compute the longitudinal river profile and SL gradient index.

K_s, the ratio of channel gradient and drainage basin area, was also utilized to identify and quantify the knick points, and we used the data of Munack et al. (2014).

RESULTS

Geomorphic setting and longitudinal river profile of the Indus River

Based on channel gradient, knick points, valley width, and channel pattern, the river was divided into four segments: segment 1, Nyoma to Mahe; segment 2, Mahe to Upshi; segment 3, Upshi to Spituk; and segment 4, Spituk to Dah (Fig. 2A). Table 1 collates the geomorphic characteristics of each segment. Valley widths in these segments are 4000 m (segment 1), 200 m (segment 2), 6000 m (segment 3), and 100 m (segment 4). The channel gradient ranged from 0.75 to 7.5 m/km (Fig. 2B).

The SL index was the lowest (490) in segment 1 and highest in segment 4 (>19,500). Noteworthy observations include the following: (1) in segment 2, although the river traversed through the same lithology (the Indus Molasse), a sudden increase in the SL index (~4500) was seen; (2) the SL decreases in segment 3 where the river flows along the contact between the Ladakh Batholith and the Indus Molasse; and (3) the SL increases in segment 4 with deformed Indus Molasse. Within this segment, the river shows a sharp increase in SL index downstream from Skyurbuchan (34°26.01′N, 76°42.90′E), from where the river flows across the Ladakh Batholith (Fig. 2C). The K_s index in segments 1 and 3 is low, whereas it is high in segments 2 and 4 (Munack et al., 2014), which suggests a definitive role of tectonics.

Sedimentation and lithofacies

We prepared 28 graphic lithological logs, and based on sediment characteristics, seven lithofacies were identified. These were coded as per Miall (1996). Table 2 presents the characteristics of individual lithofacies. The gravel lithofacies had three subfacies: (1) subfacies A, where the constituent clasts were granitic derived from the Ladakh Batholith; (2) subfacies B comprised clasts from Indus Molasse; and (3) subfacies C comprised a mixed source and represented deposition in the trunk channel. Lithofacies were grouped into two lithofacies associations and were classified as (1) channel bound sequence and (2) fan bound sequence.
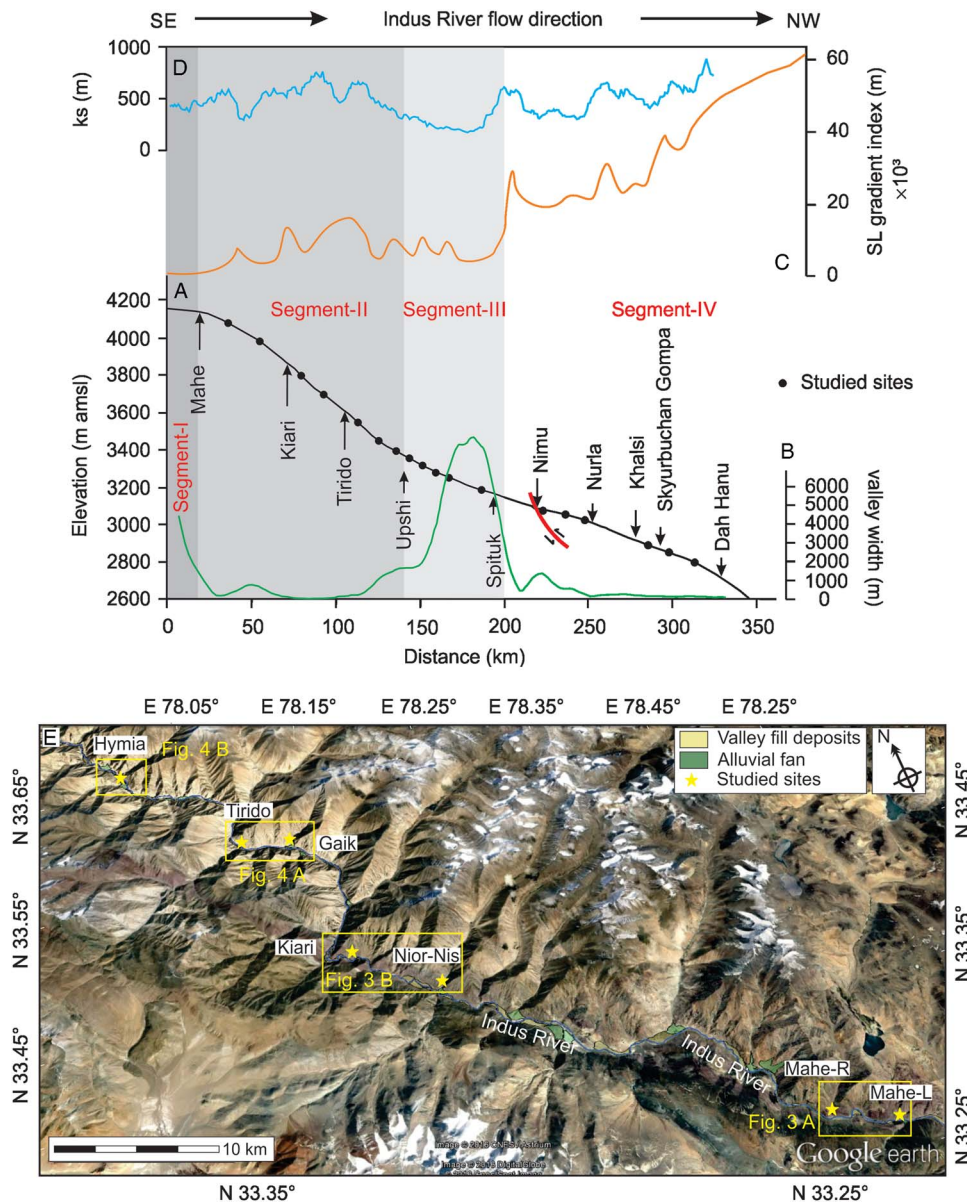
Figure 2. Longitudinal river profile (A) of Indus River valley width (B) from Mahe upstream to Dah (after Munack et al., 2014). (C) Stream length (SL) gradient index plotted along the Indus River. (D) K_s plotted along the channel (after Munack et al., 2014). Note the four segments of Indus River with distinct channel gradient and SL index. Segment 1 seems to be the southwest edge of the Tibetan plateau. (E) Google Earth image showing geomorphology along the Indus River as it flows in a narrow gorge in segment 2 (Mahe to Hymia). Note the study locations. Yellow stars locate various studied sections. The yellow rectangles are insets to Figures 3 and 4. m amsl, meters above mean sea level. (For interpretation of the references to color in this figure legend, the reader is referred to the web version of this article.)

The channel bound sequences are 2.5 to 27 m thick and up to ~50 m wide, multistoried units. Laterally, these units exhibit lensoidal geometry and fining upward trends that internally consist of clast-supported, horizontally stratified gravels (Gh), massive gravels (Gcm), planar cross-bedded gravels (Gp), and planar cross-laminated sand (Sp) lithofacies. Generally, in a vertical sequence several such units separated by a lens of horizontally laminated sand facies (Sp) is common. At places, these units are overlain or underlain by matrix-supported graded gravel (lithofacies Gmg).

The fan bound sequences are 5 to 30 m thick and comprise matrix-supported graded gravels (Gmg), matrix-supported massive gravels (Gmm), horizontally laminated sand (Sh), and planar cross-bedded sand (Sp) lithofacies. Individual units had a fining upward trend, often tabular and laterally extending over several tens to hundreds of meters. In places, they are capped by horizontal or planar cross-bedded sandy facies. The constituent gravels are angular and poorly sorted and have a single provenance (either of Ladakh Batholith or Indus Molasse).

Table 1. Valley configuration, geomorphology, and channel gradient along the Indus River.

Segment	Average channel gradient (m/km)	Valley width, minimum–maximum (m)	Description
Segment 1 (Nyoma to Mahe)	0.75	3900 ± 150	The channel pattern is braided to anastomosing with coarse to pebbly sand as bed load. The geology comprises Indus Molasse with Karakoram Fault running in the vicinity (~20 km northeast from Nyoma). At Mahe, the channel on the right bank is flanked by a gravel fill sequence.
Segment 2 (Mahe to Upshi)	7.2	110–385	From Mahe, the Indus descends into a deep and narrow gorge and shows development of one level of fill terrace. The channel is carved into Ladakh Batholith (granite and granodiorite) downstream to Kiari, whereas in the stretch in between Mahe and Kiari the host rock is Indus Molasse.
Segment 3 (Upshi to Spituk)	1.8	240–1200	In this segment, the river loses its gradient, opens up into the wide valley of Leh, and flows along the Upshi-Bazgo Thrust. Geomorphologically, this segment shows alluvial fans, amphitheater valleys, and fill terraces (Fig. 5) This segment continues a little downstream of Spituk where the river again enters into a narrow valley.
Segment 4 (downstream Spituk to Dah)	4–7.5	100–500	The Indus in most parts of this segment cuts through Indus Molasse except near Dah where it cuts into Ladakh Batholith. This segment also shows development of a fill terrace and two levels of strath terraces. Near Skyurbuchan and Dah, the gradient has increased up to 7.5 m/km.

Morphostratigraphy and OSL chronology

Morphostratigraphically, the upper Indus River could be divided into two segments: (1) from Nyoma to Spituk, characterized by varying channel gradient, a level of fill terrace (T-1), and alluvial fans; and (2) Spituk to Dah, characterized by persistence of T-1 and one or two strath terraces. In the following terrace configuration, sedimentary profiles and OSL chronology of different sections are described.

The OSL measurements indicated that most samples had poor luminescence sensitivity, were well bleached, and showed typical quartz shine down and luminescence versus dose growth curves. Preheat and dose recovery tests yielded signal stability between 200°C and 240°C. As the recuperation ratio was lowest at ~220°C, a preheat of 220°C was used. Table 3 provides OSL ages with relevant data.

Segment: Nyoma to Spituk

In this segment, 10 sections (Mahe, Niornis, Kiari, Gaik, Tirido, Hymia, Upshi, Kharu, Stakna, and Spituk) were studied to understand the sedimentary profile of fill terrace (Fig. 2E). At Mahe, where the river cuts through the Indus Molasse, a 10.5-m-thick valley fill comprised the basal 5.5 m of channel bound sediment overlain by a 5-m-thick, poorly sorted matrix-supported debris flow unit with ~90% of the constituent gravels sourced from the Indus Molasse (Fig. 3A). Two samples from this section yielded OSL ages of 41 ± 2 ka (LD-1047) and 14 ± 2 ka (LD-1433; Fig. 3A).

The section at Niornis, ~50 km downstream from Mahe, had a ~70-m-thick valley fill comprised of 20 fining upward cycles of channel bound sequence. A sample at ~40 m above the base yielded an OSL age of 28 ± 4 ka (LD-1048; Fig. 3B). Approximately 8 km farther downstream at Kiari, an 18-m-thick fill comprised the basal 5 m of alluvial fan bound debris flows mainly derived from Ladakh Batholith. These were overlain by a 13-m-thick unit of channel bound sequence of mixed lithology. A sample 12 m below the top yielded an OSL age of 26 ± 4 ka (LD-1063). From Gaik to Hymia, for ~18 km (Fig. 4), the river flows into a narrow gorge across granites of Ladakh Batholith. At Gaik, a 42-m-thick fill sequence comprised the basal 24 m of channel bound sequence of mixed lithology followed by 11 m of alluvial fan bound sequence with source in Ladakh Batholith and a 7-m-thick unit of channel bound sequence (Fig. 4A). Two samples at 20 (basal channel bound unit) and 7 m below the surface (top of the fan sequence) yielded OSL ages of 13 ± 1 ka (LD-1064) and 15 ± 1 ka (LD-1065).

Approximately 9 km downstream at Tirido, a 24.5-m-thick section comprised two units of channel bound sequence of mixed lithology, and two samples at 16 and 0.5 m depth yielded OSL ages of 29 ± 3 ka (LD-1066) and 26 ± 2 ka (LD-1067), respectively (Fig. 4A). At Hymia, ~14 km farther downstream from Tirido (Fig. 4B), a 14-m-thick section comprising the basal 2.5 m channel bound sequence was overlain by a 2.5-m-thick unit of alluvial fan bound sequence and ~9 m of channel bound sequence. Samples from the base and another at a depth of 7 m have ages of 23 ± 1 ka (LD-1069) and 24 ± 1 ka (LD-1068).

Downstream from Hymia, the low gradient channel is flanked by (1) steeply dipping alluvial fans emerging from the Indus Molasse (Zanskar ranges; Drew, 1873), (2) low gradient

Table 2. Lithofacies, subfacies, description, and interpretation.

Facies	Description	Interpretation
Clast-supported, horizontally stratified imbricated gravels (Gh)	Composed of well-rounded, moderately well-sorted, and imbricated clasts. Clast size ranges from 4 to 50 cm. Individual units are 0.5 m to a few meters thick, multistoried, vertically fining upward. Laterally, these are sheet to lensoid in shape, with lateral extent of ~50 m. Matrix ranges between 10% and 30%.	This lithofacies represents deposition on a channel bar, and based on sediment composition, it is identifiable as subfacies A, B, and C.
Clast-supported massive gravels (Gcm)	Made up of 1- to 10-m-thick well-rounded, moderately well-sorted, clast-supported massive gravels. Clast size ranges from 3 to 80 cm. Laterally, this facies occurs as a lensoid of ~30 m width. The matrix is gray to dark gray in color, and fine to coarse sand with granules constitutes 10%–20% of the bulk volume.	Amalgamation of channel bar during riverbed accretion developed Gcm facies; suggests a low-strength laminar to turbulent flow. Successive flood events erode upper few centimeters of previously deposited fluvial unit and deposit new sediment in the form of Gcm facies (Shukla, 2009).
Matrix-supported graded gravels (Gmg)	Subangular to poorly rounded, moderately to poorly sorted, matrix-supported graded gravels. Gravel size is 5–55 cm thick, and individual units range from 0.35 to 3 m. The matrix, medium to gritty sand, is up to 40% of the volume. The individual unit often grades upward into sand units that indicate termination of a flood event.	This unit is deposited by high-energy plastic debris flow where the clasts are suspended in the plastic silty-sand medium with low water concentration and represent episodic flood events (Ray and Srivastava, 2010).
Matrix-supported massive gravels (Gmm)	This facies included subangular to poorly rounded, poorly sorted, matrix-supported massive gravels. Clast size is 5–100 cm thick, and units range from 2 to 6 m. Matrix: medium to gritty sand, contributes ~40%–50% of the total volume. This unit is massive and has erosional contact with lower as well as upper unit.	This unit indicates a high-energy plastic debris flow (Ray and Srivastava, 2010).
Clast-supported, planar cross-bedded gravels (Gp)	This is composed of 1- to 3-m-thick, well-rounded, moderately to well-sorted, planar cross-bedded gravels, identifiable as subfacies A and B. Gravel size ranges between 5 and 10 cm in diameter and forms cross beds with toe angle of 10°–15°. Internally, it makes cosets of finning upward units capped by sandy lenses and invariably has basal erosional contact. The matrix is ~10% and is medium and pebbly sand.	This lithofacies is formed by migration of high-relief two-dimensional (2-D) bed forms in a channelized flow (Miall, 1996) with a velocity of 2–3 m/s forming channel bars.
Horizontally laminated sand (Sh)	This is composed of 0.25- to 3-m-thick, horizontally bedded, parallel laminated units of coarse to fine sand. The individual lamina is 1–2 mm thick. Occurred in sheet or lensoid geometry and laterally extended up to ~20 m.	This facies occurred in association with the gravel facies. This lithofacies is deposited on the top of the channel bars under waning flood conditions.
Planar cross-bedded sand (Sp)	Grayish-colored, 0.30- to 4-m-thick, planar cross-bedded medium to coarse sand. Individual laminas 2–5 mm thick. Laterally, the units are lenticular in shape having a width of 2–10 m.	The planar cross-bedded sand facies is formed by the movement of 2-D bed forms on a channel bar.

amphitheaters of deglaciated valleys draining the Ladakh Batholith, and (3) valley fill terraces (Fig. 5A). Toward the toe of alluvial fans, a flatter terrace, T-1, rests on the modern riverbank. A 38-m-thick section at Upshi (Upshi-R; Fig. 5B) comprised the basal ~30 m channel bound sequence of mixed lithology with an OSL age of 37 ± 3 ka (LD-1070; Fig. 5B). An 8-m-thick alluvial fan bound unit sourced from the Ladakh Batholith overlay this. At Upshi-L, a 26-m-thick section (Fig. 5C) on the southern bank of the river comprised the basal 15-m-thick, mixed sourced channel bound sequence whose top was OSL dated to 30 ± 2 ka (LD-1046; Fig. 5C). This was overlain by an 11-m-thick unit of molasse sourced alluvial fan deposit. The upper alluvial fan event was traceable to 12 km

downstream at Kharu where it made an ~30-m-thick section. The top of this section had an OSL age of 33 ± 2 ka (LD-1045; Fig. 5D).

Similarly, at Stakna (Fig. 5E), valley fill terrace sections comprised three depositional units (Figs. 5E). The basal 4 m of this unit comprised alluvial fan bound sediments sourced from molasse rocks. This had an OSL age of 47 ± 1 ka (LD-1015). This unit was overlain by a 3-m-thick channel bound unit made up of gravels of mixed lithology with an OSL age of 28 ± 1 ka (LD-1016). A 5 m debris flow unit above this was OSL dated to 25 ± 1 ka (Stakna, LD-1044; Fig. 5E).

At Stakna-1, a 12-m-thick section comprised the basal 1 m channel bound sequence overlain by an ~11-m-thick alluvial

Table 3. Sample location, dosimetry, paleodose, dose rate, and ages of all the samples collected from the Indus River.

Lab no.	Field name	Latitude	Longitude	Depth (m)	U (ppm)	Th (ppm)	K (%)	Cosmic dose rate (μGy/a)	Weighted mean paleodose (Gy)	Dose rate (Gy/a)	Mean age (ka)
Mahe											
LD-1433	IR-1	33°16.09′N	78°28.12′E	9.63	3.17	5.2	1.9	254 ± 76	42 ± 7	3.1 ± 0.1	14 ± 2
LD-1047	IND-15	33°17.06′N	78°25.27′E	8	2.5	10.1	2.4	274 ± 81	154 ± 6	3.8 ± 0.1	41 ± 2
Niornis											
LD-1048	IND-16	33°25.97′N	78°11.93′E	5	8.6	9.3	2.7	299 ± 90	106 ± 15	3.8 ± 0.2	28 ± 4
Kiari											
LD-1063	IND-17	33°28.19′N	78°8.67′E	12	2.3	8	2.2	241 ± 72	88 ± 12	3.4 ± 0.2	26 ± 4
Gaik											
LD-1064	IND-18	33°34.28′N	78°7.53′E	20	4.1	11	2.6	217 ± 65	58 ± 5	4.4 ± 0.2	13 ± 1
LD-1065	IND-19	33°34.28′N	78°7.53′E	7	3.5	16.1	2.9	268 ± 80	74 ± 7	4.9 ± 0.2	15 ± 1
Tirido											
LD-1066	IND-20	33°35.07′N	78°4.96′E	16	2.9	8.5	2.1	223 ± 67	100 ± 12	3.5 ± 0.2	29 ± 3
LD-1067	IND-21	33°35.07′N	78°4.96′E	0.5	2.5	5.6	2.5	372 ± 112	102 ± 6	3.7 ± 0.2	26 ± 2
Hymia											
LD-1068	IND-22	33°39.98′N	77°59.74′E	7	2.2	15	3.1	260 ± 78	117 ± 5	4.7 ± 0.2	24 ± 1
LD-1069	IND-23	33°39.98′N	77°59.74′E	13.5	2.9	13.4	2.3	225 ± 68	91 ± 7	4.0 ± 0.2	23 ± 2
Upshi											
LD-1070	IND-24	33°47.37′N	77°51.14′E	10	1.4	7.7	1.6	237 ± 71	108 ± 8	2.9 ± 0.1	37 ± 3
LD-1046	IND-14	33°49.82′N	77°48.76′E	15	2.3	21.1	2.7	212 ± 63	145 ± 7	4.8 ± 0.2	30 ± 2
Kharu											
LD-1045	IND-13	33°54.95′N	77°44.07′E	3	2.0	12.1	2.6	295 ± 89	131 ± 6	4.0 ± 0.2	33 ± 2
Stakna											
LD-1015	IND-8	33°57.51′N	77°42.77′E	7	1.5	7.9	1.9	245 ± 75	137 ± 4	2.9 ± 0.2	47 ± 1
LD-1016	IND-9	33°57.51′N	77°42.77′E	5	2.2	10.7	2.1	264 ± 78	98 ± 4	3.5 ± 0.1	28 ± 1
LD-1044	IND-12	33°57.59′N	77°42.96′E	3	2.7	16.4	2.9	292 ± 87	121 ± 7	4.8 ± 0.2	25 ± 1
Stakna 1											
LD-1017	IND-10	33°57.59′N	77°42.96′E	8	2.6	11.8	2.0	238 ± 72	103 ± 5	3.5 ± 0.1	29 ± 1
LD-1043	IND-11	33°57.59′N	77°42.96′E	3.5	1.1	8.6	1.8	264 ± 78	84 ± 4	2.8 ± 0.1	30 ± 1
Stakna 2											
LD-985	IND-25	34°0.18′N	77°41.74′E	10	1.9	8.3	1.6	226 ± 68	89 ± 23	2.9 ± 0.1	31 ± 8
LD-986	IND-26	34°0.18′N	77°41.74′E	11	4.0	8.9	1.7	221 ± 66	157 ± 24	3.4 ± 0.1	46 ± 7
Spituk											
LD-1003	IND-47	34°7.84′N	77°03.51′E	18	1.1	8.5	1.8	199 ± 60	130 ± 10	2.5 ± 0.1	52 ± 4
Nimu											
LD-1221	ZIC-1	34°9.96′N	77°19.33′E	8	1.9	6.2	0.7	200 ± 60	94 ± 10	1.7 ± 0.1	55 ± 6
Saspol											
LD-1000	IND-44	34°14.84′N	77°6.68′E	10	1.3	7	1.9	217 ± 66	48 ± 5	2.8 ± 0.1	17 ± 2
LD-990	IND-43	34°14.84′N	77°6.68′E	11.25	1.5	11.1	1.6	211 ± 63	140 ± 13	2.8 ± 0.1	50 ± 5
Nurla											
LD-989	IND-42	34°17.40′N	77°2.06′E	20	1.2	6.3	0.9	187 ± 57	133 ± 9	1.7 ± 0.1	78 ± 5

Table 3. (*Continued*)

Lab no.	Field name	Latitude	Longitude	Depth (m)	U (ppm)	Th (ppm)	K (%)	Cosmic dose rate (μGy/a)	Weighted mean paleodose (Gy)	Dose rate (Gy/a)	Mean age (ka)
Khalsi											
LD-997	IND-39	34°19.56′N	76°50.67′E	30	1.0	12.2	1.5	179±54	140±13	2.7±0.1	52±5
LD-996	IND-38	34°19.56′N	76°50.67′E	1.5	0.7	6.4	1.4	301±90	90±8	2.2±0.1	41±4
LD-998	IND-40	34°19.56′N	76°50.67′E	4	1.3	7.6	2.1	260±78	55±4	3.1±0.1	18±1
Dumkhar											
LD-995	IND-37	34°23.97′N	76°45.83′E	9	1.2	12.9	1.7	217±66	170±9	3.0±0.1	57±3
Skyurbuchan Gompa											
LD-988	IND-36	34°26.01′N	76°42.90′E	15	1.5	7	2.0	195±60	163±21	2.9±0.1	56±7
Skyurbuchan Downstream											
LD-987	IND-33	34°27.01′N	76°41.09′E	19	1.2	6.7	1.1	187±57	149±12	1.8±0.1	83±7
LD-993	IND-34	34°27.01′N	76°41.09′E	4.5	1.3	8.3	1.5	253±75	117±17	2.5±0.1	47±7
Biamah											
LD-991	IND-31	34°36.58′N	76°29.97′E	6.5	2.1	12.4	1.4	226±69	21±3	2.9±0.1	7±1

fan bound sequence sourced from the batholith. These had OSL ages of 29 ± 1 ka (LD-1017) and 30 ± 1 ka (Stakna-1, LD-1043; Fig. 5E).

The third section, ~5 km downstream of Stakna (Stakna-2), on the northern bank, represents a relict alluvial fan prograding from the Ladakh Batholith. This had a 49-m-thick sequence of channel bound, partially weathered, pale-yellow granitic gravels and comprised two depositional events. The basal event was dated to 46 ± 4 ka (Stakna-2, LD-986; Fig. 5E), and the upper to 31 ± 1 ka (LD-985).

At the western Leh at Spituk (34°07.13′N, 77°30.66′E), an ~45-m-thick section was exposed on the northern bank of the river valley (Fig. 5F). The lower ~10 m comprised channel bound sediments with intervening, ~1-m-thick lensoidal bodies of massive, brown coarse sand sourced from the Indus Molasse. This was overlain by 30-m-thick lacustrine sediments followed by ~5 m of eolian sand toward the top. A sample from the bottom gray sand unit yielded an OSL age of 52 ± 4 ka (LD-1003; Fig. 5F), and that from the topmost eolian unit yielded an OSL age of 20 ± 2 ka (Kumar et al., 2016). Similarly, a 36.5-m-thick section located on the left bank at Spituk had ~30 m of alluvial fan deposit at its base, also sourced from the Indus Molasse. The sequence comprised more than 20 units of matrix-supported angular clast lithofacies and was overlain by 2.8-m-thick lacustrine deposits.

Segment: Nimu to Dah

This ~120 km stretch of the Indus River traverses a gorge and exhibits strath and valley fill terraces (see Fig. 6A; Table 4). At Nimu, at the confluence of the Indus and Zanskar Rivers (34°09.81′N, 77°20.15′E), a valley fill terrace (T-1) and a strath terrace (T-2) are present (Fig. 6B). The fill terrace comprised an ~12-m-thick channel bound sequence and the strath terrace T-2 at 124 ± 6.2 m arl (Fig. 6C). This was overlain by a 12.5-m-thick sequence of channel bound sediments. The strath terrace exhibited entrenched meander topography, and a sample from the youngest meander yielded an OSL age of 55 ± 6 ka (LD-1221; Fig. 6C). Blöthe et al. (2014) dated an older meander of this terrace to 206 ka using cosmogenic [10]Be. The OSL age implies a bedrock incision rate of 2.2 ± 0.4 mm/a.

About 29 km downstream from Nimu, at Saspol (34°14.84′N, 77°6.46′E) (Fig. 6D, Table 4), the river cuts through the Indus Molasse and two terraces, T-1 and T-2. T-1 comprised 19-m-thick channel bound sediments, and a sample at 10 m below the surface gave an OSL age of 17 ± 2 ka (T-1, LD-1000; Fig. 6D). Strath terrace T-2 was at 81.2 ± 4 m arl and was covered by 17 m of channel bound sediments. A sample at a depth of 11.5 m yielded an OSL age of 50 ± 5 ka (T-2; Fig. 6D). Terrace T-2 can be traced downstream for ~1 km, yielding a bedrock incision rate of 1.6 ± 0.2 mm/a.

At Nurla, ~10 km downstream of Saspol, a former meander of the Indus River is present on the north bank of the river (Fig. 7A). The strath terrace relating to this meander was at 148 ± 7.4 m arl and had a 20-m-thick alluvial cover. A
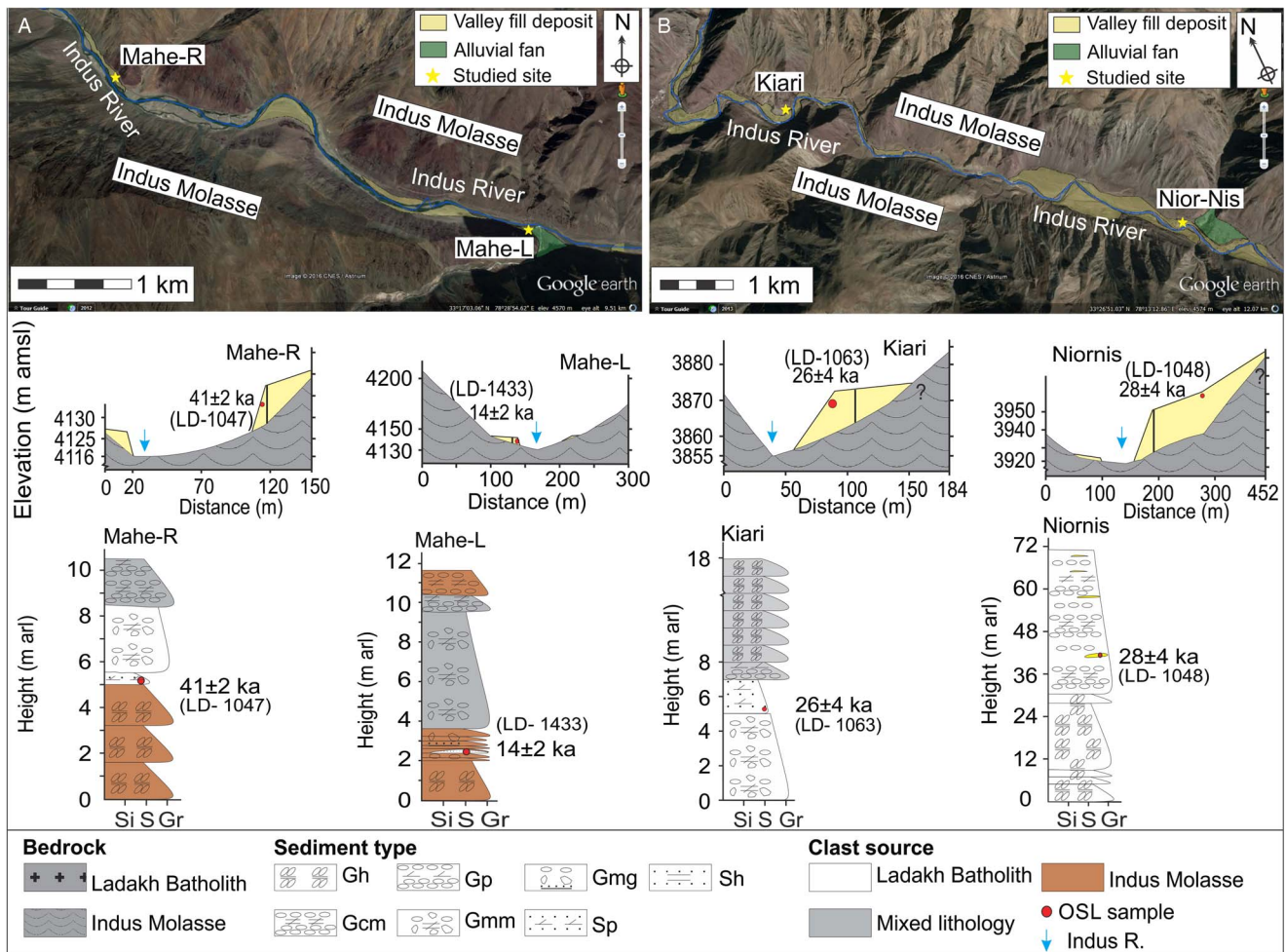
Figure 3. (color online) The Google Earth image showing the studied sections Mahe-L and Mahe-R (A) and Niornis (B). Lower panel shows the morphostratigraphy and luminescence chronology of these sections. m amsl, meters above mean sea level; m arl, meters above river level.

sample near the bottom gave an OSL age of 78 ± 5 ka (LD--989; Fig. 7B). The estimated bedrock incision rate here was 1.9 ± 0.2 mm/a. Approximately 20 km further downstream at Khalsi, the river continues to flow through the Indus Molasse and has three terraces: T-1, T-2', and T-2 (Fig. 7C, Table 4). Terrace T-1 comprised a 31.2-m-thick channel bound sequence, and a sample near the top yielded an age of 18 ± 1 ka (T-1, LD-998; Fig. 7C). Strath terrace T-2', at an elevation of 50.2 ± 2.5 m arl, had a 7-m-thick sediment and dated to 41 ± 4 ka (T-2', LD-996; Fig. 7C). The uppermost terrace, T-2, at 158.8 ± 8 m arl had an ~20-m-thick cover of channel bound sequence, which was OSL dated to 52 ± 5 ka (T-2, LD-997; Fig. 7C and D). The bedrock incision rate from T-2 was 3.0 ± 0.4 mm/a and from T-2' was 1.2 ± 0.2 mm/a.

The stretch between Dumkhar and Skyurbachan Gompa has a fill terrace T-1 and a strath terrace T-2 (Fig. 8A). At Dumkhar (Fig. 8B), a valley fill terrace (T-1) comprised a 33.3-m-thick channel bound sediment followed by a strath terrace (T-2) at an elevation of 132.5 ± 6.6 m (arl) overlain by 18-m-thick channel bound gravel (Fig. 8B). A sample from the fluvial gravel of terrace T-2 yielded an OSL age of

57 ± 3 ka (LD-995) and provided a bedrock incision rate of 2.3 ± 0.2 mm/a. This terrace configuration continues for another 6.5 km, and at Skyurbuchan Gompa terrace T-2 was at 142.5 ± 7 m (arl) and overlain by 15.5 m of fluvial gravels (Fig. 8C, Table 4). The base of the overlying gravels yielded an OSL age of 56 ± 7 ka (LD-988) and thereby provided an bedrock incision rate of 2.5 ± 0.4 mm/a. Similarly, ~5 km downstream of Skyurbachan Gompa, a 25-m-thick, scree-covered fill terrace (T-1) and two strath terraces (T-2' and T-2) at elevations of 40 ± 2 m (arl) and 150 ± 7.5 (arl) were present. The alluvial cover of T-2' and T-2 were OSL dated to 47 ± 7 (LD-993) and 83 ± 7 ka (LD-987; Fig. 8D) and yielded bedrock incision rates of 0.85 ± 0.2 and 1.8 ± 0.2 mm/a, respectively.

Downstream from there, the river flows through the Ladakh Batholith and carves a deep and narrow gorge with only one level of fill terrace. A sediment fill of 17 m thickness at Biamah and 15 m at Dah, ~35 km farther downstream, was noted. A debris flow sample from the top of the sequence at Biamah yielded an OSL age of 7 ± 1 ka (LD-991; Table 1). The strath height, ages of the alluvial cover, and estimated bedrock incision rates are collated in the Table 4.
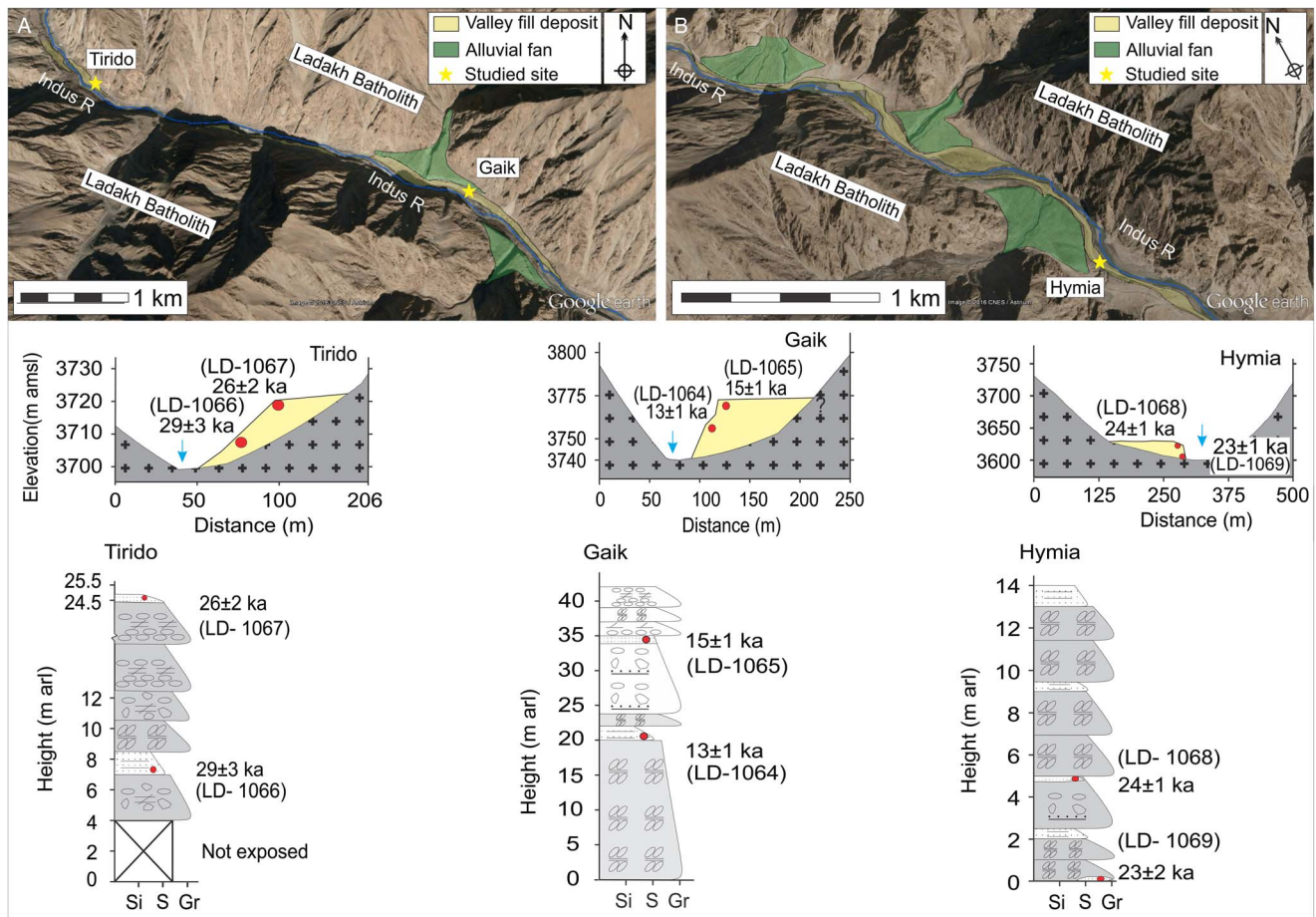
Figure 4. (color online) The Google Earth image showing the studied sections Gaik and Tirido (A) and Hymia (B). Lower panel shows the morphostratigraphy and luminescence chronology of these sections. m amsl, meters above mean sea level; m arl, meters above river level.

DISCUSSION

Sedimentation pattern and paleoclimate

Sedimentation pattern and aggradation in a river valley depends on the relative proportions of water and sediment in the channel network, vegetation cover, and the system state with respect to its being supply or transport limited (Blum and Törnqvist, 2000; Srivastava et al., 2008). The sediment load of a channel depends on contemporary climate and relief, driven by tectonics. Most of the stretch from Mahe to Dah exhibited widespread valley fills in the form of terrace T-1 and alluvial fan sequences. The stratigraphy of terrace T-1 and alluvial covers of strath terraces suggest that channel bound and alluvial fan bound debris flows controlled the aggradation in the valley. Lithofacies composition (Gh, Gp) of channel bound deposits suggests that the traction current-mediated processes resulted in the aggradation of channel bars. Internally, these bars comprised large-scale planar two-dimensional bed forms suggestive of sustained flood conditions with broad hydrograph, characteristic of wetter conditions (Miall, 1996; Suresh et al., 2007; Shukla, 2009; Ray and Srivastava, 2010). Fan bound deposits

represented tributary or outwash alluvial fan aggradation via sheet type, nonchannelized floods originating from the glaciers or from flash floods (Srivastava et al., 2013). Intercalations of these two types of sequences suggest deposition under subhumid-paraglacial climates where the trunk channel flooded regularly and the channel bars aggraded vertically and episodically because of high sediment supply from glacier-fed tributaries that brought sediments via flash floods (Miall, 1996). Nearly 50% of the cumulative thickness of the sequences were channel bound gravels of subfacies C and comprised homogenized multiprovenance sediments. The remaining 50% was of a single provenance (subfacies A and B). This indicates that, although regular floods in the Indus River that fetch sediment from all over the catchment were responsible for aggradation, the sediment supplied by tributaries via episodic discharge was of equal importance.

The Spituk lake sequence on the alluvial fan emanating from molasses suggests that (1) this sequence postdated the alluvial fans, and (2) the paleolake formed by progradation of fans, both from the Ladakh Batholith and the Indus Molasse. Detailed sedimentary architecture of this sequence and the surrounding area presented by Sinclair et al. (2017) indicates that neotectonically forced northeastward movement of the
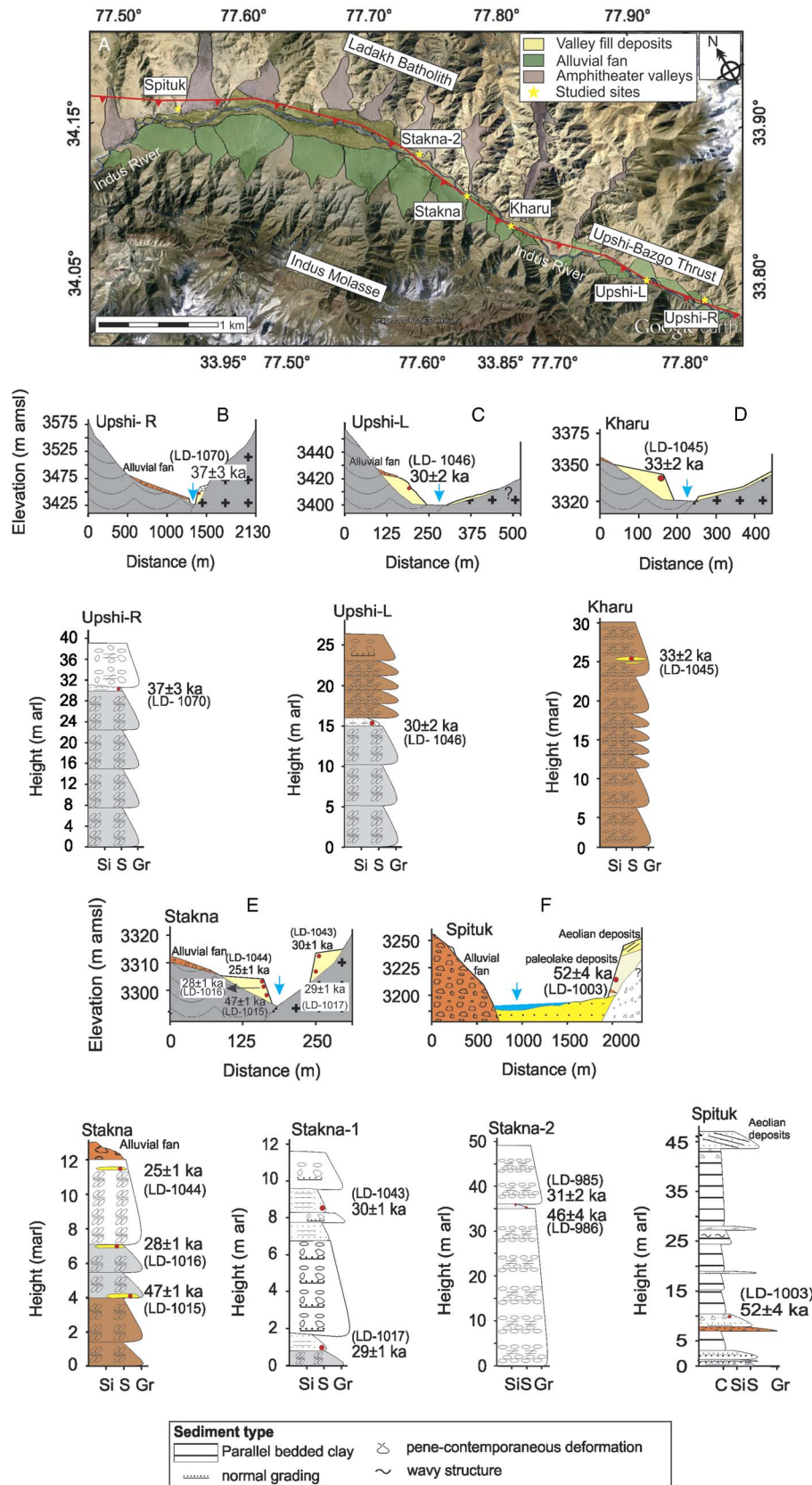
Figure 5. (A) Geomorphology of segment 3 around Leh (Upshi to Spituk). Note the alluvial fans sourced from Indus Molasse and amphitheaters from Ladakh Batholith. The red line with triangles shows the traverse of Upshi-Bazgo Thrust. Valley cross section, morphostratigraphy, and lithologs of fill terraces of studied sections at Upshi-R (B), Upshi-L (C), Kharu (D), Stakna (E), and Spituk (F). m amsl, meters above mean sea level; m arl, meters above river level. (For interpretation of the references to color in this figure legend, the reader is referred to the web version of this article.)
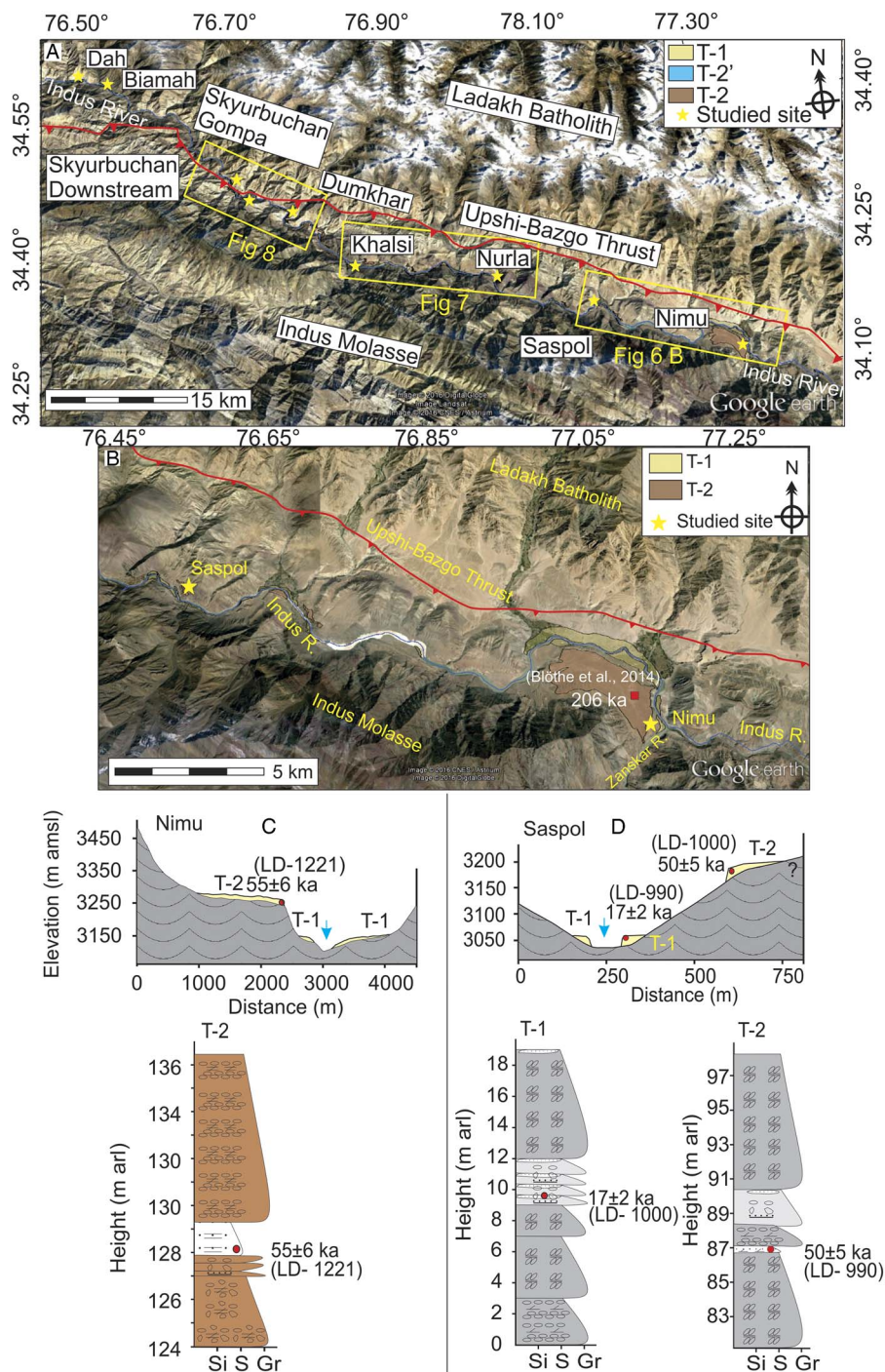
Figure 6. (A) Google Earth image showing segment 4 of the Indus River from Nimu to Dah. The studied sections are marked by yellow stars. The contact between Indus Molasse and Ladakh Batholith is marked by a red line with triangles. The yellow rectangles are the insets for Figures 6B, 7, and 8. (B) Terraces between Nimu and Saspol. Note one level of fill terrace T-1 (yellow) and strath terraces T-2 (brown). The Indus River flowing in the narrow gorge carved into Indus Molasse. Geomorphology at Nimu and Saspol sections. Note the incised meander at Nimu section and sampling locations of Blöthe et al. (2014) and this work. Valley cross section and morphostratigraphy and lithologs of fills at Nimu (C) and Saspol (D) indicating one level of filled and one level of strath terrace. m amsl, meters above mean sea level; m arl, meters above river level. (For interpretation of the references to color in this figure legend, the reader is referred to the web version of this article.)

Indus River controlled the sedimentary architecture of the valley at Spituk, and the Stok Thrust played an active role.

The present work suggests that the sediments at Spituk were deposited between 52 and >20 ka. Sinclair et al. (2017) OSL dated the upper part of the Spituk section to 27 ± 3 ka, which falls within this age bracket. Previously, infrared-stimulated luminescence ages of 177–72 ka (Blöthe et al., 2014) and ^{14}C–accelerator mass spectrometry ages of 10–1.5 ka (Phartiyal

Table 4. Terrace configuration (e.g., fill or strath type), thickness of fill and strath above the river level (arl), chronology, and bedrock incision rates as studied along the Indus River.

Section no.	Location	Latitude	Longitude	Elevation (m)	Type of terrace	Thicknessarl (m)	Chronology (ka)	Bedrock incision rates (mm/a)
Nyoma to Spituk segment								
1	Mahe	33°17.06′N	78°25.27′E	4116	Fill terrace	T-1: 10.5	14–41	–
2	Niornis	33°25.97′N	78°11.93′E	3920	Fill terrace	T-1: 70	28 ± 4	–
3	Kiari	33°28.19′N	78°8.67′E	3855	Fill terrace	T-1: 18	26 ± 4	–
4	Gaik	33°34.28′N	78°7.53′E	3746	Fill terrace	T-1: 42	13–15	–
5	Tirido	33°35.07′N	78°4.96′E	3705	Fill terrace	T-1: 24.5	26–29	–
6	Hymia	33°39.98′N	77°59.74′E	3605	Fill terrace	T-1: 14	23–25	–
7	Upshi R	33°47.37′N	77°51.14′E	3429	Fill terrace	T-1: 38	37 ± 3	–
	Upshi L	33°39.98′N	77°59.74′E	3397	Fill terrace	T-1: 26	30 ± 2	–
8	Kharu	33°54.95′N	77°44.07′E	3327	Fill terrace	T-1: 30	33 ± 2	–
9	Stakna 1	33°57.51′N	77°42.77′E	3305	Fill terrace	T-1: 13	25–47	–
	Stakna 2	33°57.59′N	77°42.96′E	3305	Fill terrace	T-1: 12	29–30	–
	Stakna 3	34°0.18′N	77°41.74′E	3280	Fill terrace	T-1: 49	31–46	–
10	Spituk	34°7.84′N	77°03.51′E	3185	Fill terrace	T-1: 45	52 ± 4	–
Nimu to Dah segment								
11	Nimu	34°9.96′N	77°19.33′E	3108	Strath terrace	T-2: 124 ± 6.2	T-2: 55 ± 6	2.2 ± 0.4
					Fill terrace	T-1: 12		
12	Saspol	34°14.84′N	77°6.68′E	3040	Strath terrace	T-2: 81.2 ± 4	T-2: 50 ± 5	1.6 ± 0.2
					Fill terrace	T-1: 1	T-1: 17 ± 2	
13	Nurla	34°17.40′N	77°2.06′E	3005	Strath terrace	T-2: 148 ± 7.4	T-2: 78 ± 5	1.9 ± 0.2
14	Khalsi	34°19.56′N	76°50.67′E	2939	Strath terrace	T-2: 158.8 ± 8	T-2: 52 ± 5	3.0 ± 0.4
					Strath terrace	T-2': 50.2 ± 2.5	T-2': 41 ± 4	1.2 ± 0.2
					Fill terrace	T-1: 31.2	T-1: 18 ± 1	
15	Dumkhar	34°23.97′N	76°45.83′E	2904	Strath terrace	T-2: 132.5 ± 6.6	T-2: 57 ± 3	2.3 ± 0.2
					Fill terrace	T-1: 33.3		
16	Skyurbuchan Gompa	34°26.01′N	76°42.90′E	2880	Strath terrace	T-2: 142.5 ± 7	T-2: 56 ± 7	2.5 ± 0.4
					Fill terrace	T-1: 31		
17	Skyurbuchan Downstream	34°27.01′N	76°41.09′E	2850	Strath terrace	T-2: 150 ± 7.5	T-2: 83 ± 7	1.8 ± 0.2
					Strath terrace	T-2': 40 ± 2	T-2': 47 ± 7	0.85 ± 0.2
					Fill terrace	T-1: 25		
18	Biamah	34°36.58′N	76°29.97′E	2720	Fill terrace	T-1: 17	7 ± 1	–
19	Dah	34°37.97′N	76°27.41′E	2650	Fill terrace	T-1: 15	–	–

A. Kumar and P. Srivastava
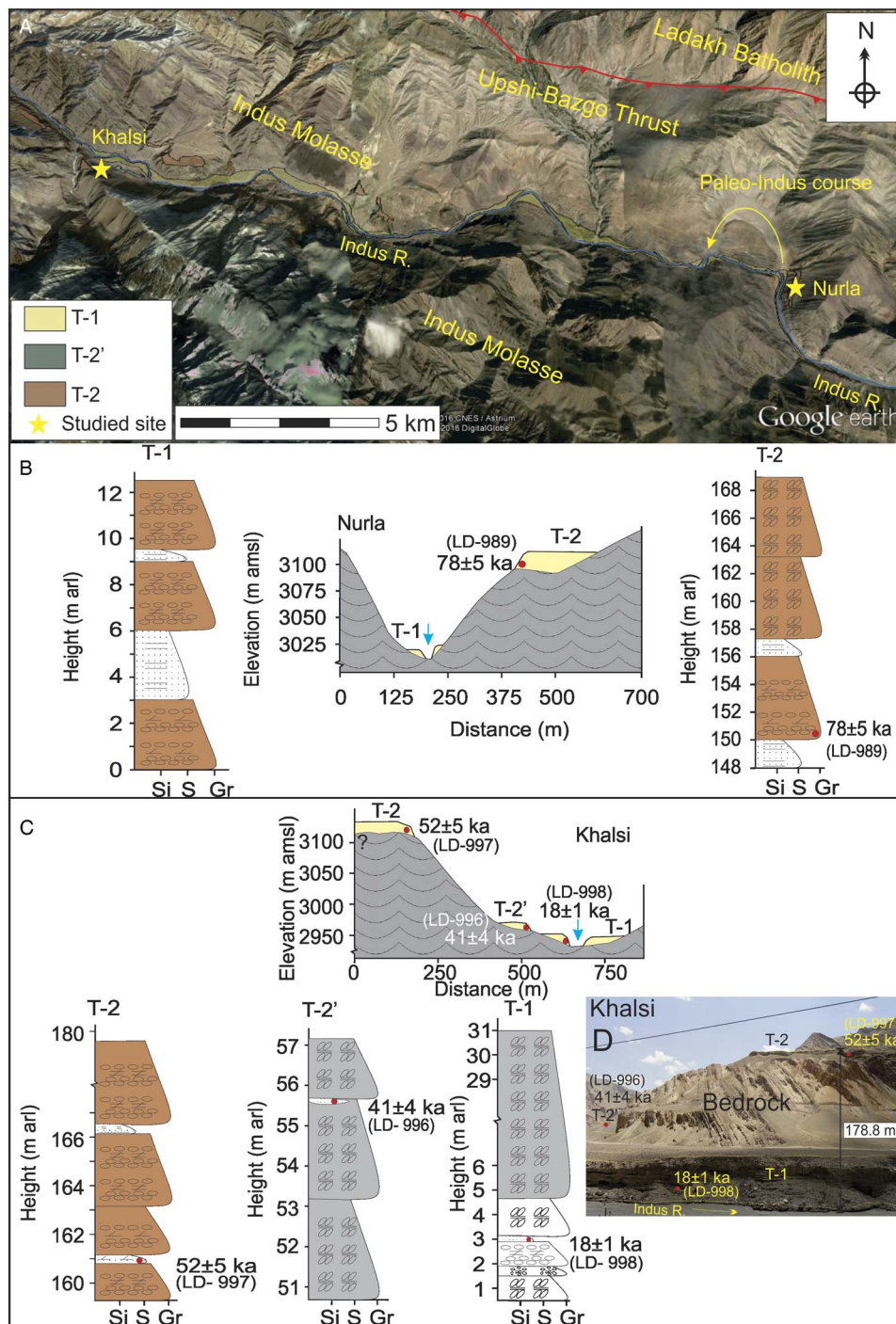
Figure 7. (color online) (A) Google Earth image showing the fill and strath terraces from Nurla to Khalsi. Note the presence of paleomeander of Indus and the corresponding strath surface at Nurla. Morphostratigraphy and chronology of Nurla (B) and Khalsi (C). (D) Field photograph of section at Khalsi showing one level of fill and two levels of strath terraces. m amsl, meters above mean sea level; m arl, meters above river level.

et al., 2013) were considered unreliable because of the possibility of incomplete bleaching of feldspar in lacustrine environments and contamination of carbon by meteoric waters.

Understanding the aggradation record in terms of climate requires analysis of the contemporary climates of the region. The records suggest the following: (1) five glacial advances in the Leh region since 430 ka (Owen et al., 2005; Ali and

Juyal, 2013; Dortch et al., 2013); (2) stronger monsoon conditions during 60–30 ka and weaker monsoon conditions during 25–18 ka as evidenced from the Guliya Ice Core, located ~400 km northeast (NE) of the study area (Fig. 9A; Thompson et al., 1997); and (3) penetration of the SW monsoon to up to >75 km beyond the orographic barrier during 14–9 ka and 50–30 ka, as well as its role in assisting
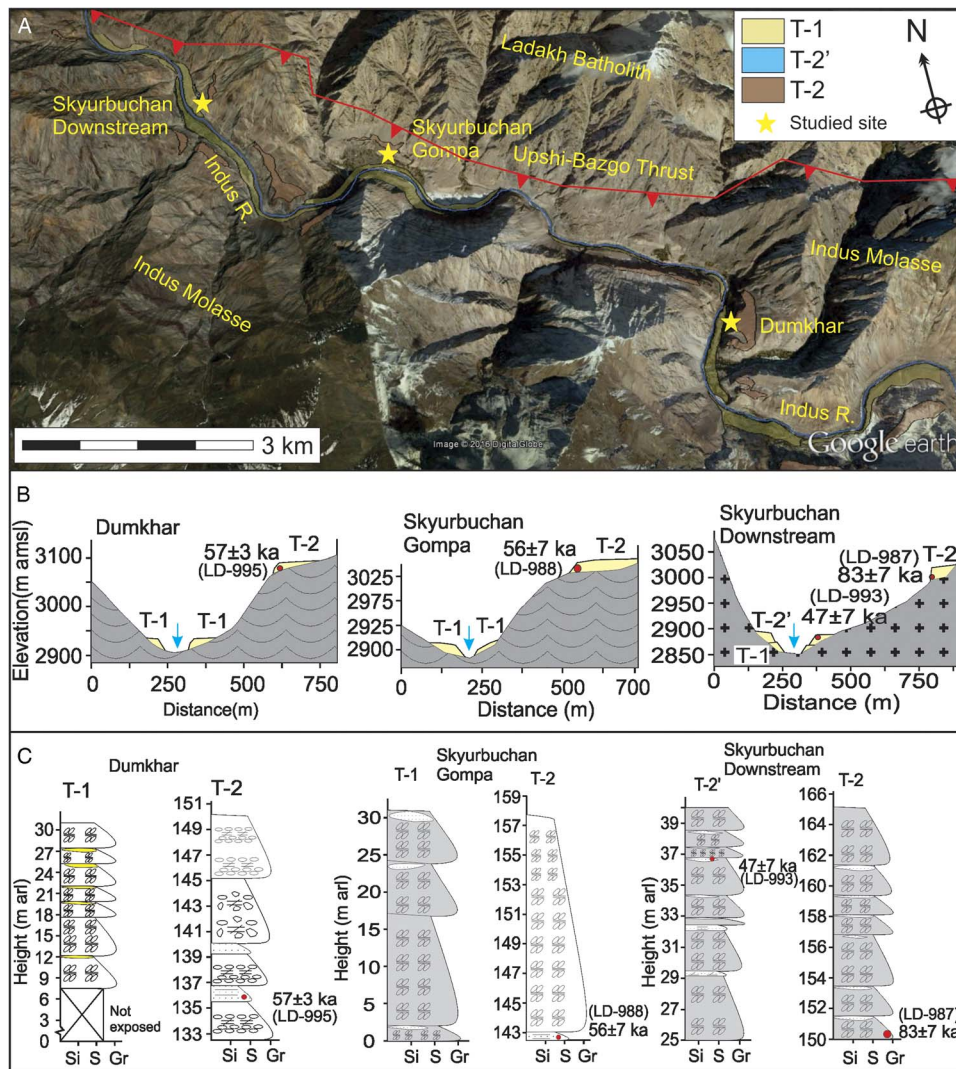
Figure 8. (color online) (A) Google Earth map showing the strath terrace located on the hanging block of Upshi-Bazgo Thrust. Valley cross section, terrace configuration, and litchologs and chronology at Dumkhar, Skyurbuchan Gompa, and Skyurbuchan Downstream sections by elevation (B) and height (C). m amsl, meters above mean sea level; m arl, meters above river level.

hill slope erosion, accentuating landslides, and enhancing the sediment budget of rivers (Bookhagen et al., 2005, Dortch et al., 2009; Srivastava et al., 2013). This is evidenced in the lacustrine and glacial records from Ladakh and Tibet that indicate postglacial warming culminating at the Holocene climatic optimum (Prell and Kutzbach, 1987; Fang, 1991; Shi et al., 2001; Owen et al., 2006a, 2008; Jung et al., 2009, 2010; Wünnemann et al., 2010; Dortch et al., 2013; Owen and Dortch, 2014; Rawat et al., 2015a, 2015b; Fig. 9B).

A comparison of OSL ages from fluvial fill (related to both T-1 and T-2), outwash fans, and debris flows with past climate records indicates that valley alluviation occurred in three pulses at 52, 28, and ~16 ka (Fig. 9C and D). Aggradation on fans occurred from ~47 to 29 ka, and three debris flow events occurred at ~27 ka. All these were suggested periods of stronger monsoon conditions. Records from the Zanskar River suggest valley aggradation between 50 and 20 ka (Blöthe et al., 2014). Thus, the phases of higher rainfall during 60–30 ka and 10–5 ka

mobilized the sediment from the catchment into the channel and assisted aggradation. It is noteworthy that river aggradation chronologies of rivers across the Himalaya—namely, Spiti, Sutlej, and Alaknanda (NW Himalaya); Marsyandi (central Himalaya, Nepal); and Brahmaputra (NE Himalaya)—that derive moisture largely from the SW Indian monsoon also experienced valley aggradation during 60–30 ka and ~10–5 ka (Pratt-Sitaula et al., 2004; Srivastava et al., 2009, 2013; Juyal et al., 2010; Ray and Srivastava, 2010; Sharma et al., 2016a).

In the NW Himalaya, two rainfall-induced phases of increased landslides are reported during 37–29 and 15–3 ka (Dortch et al., 2009). Rivers in northern Tibet in the Kunlun Mountains also built large outwash fans during ~30 ka (Owen et al., 2006b). Therefore, we conclude that on a regional scale the rivers flowing in the drier part of the Himalaya aggraded during the phases of stronger monsoon conditions. Further, when the catchment had a higher
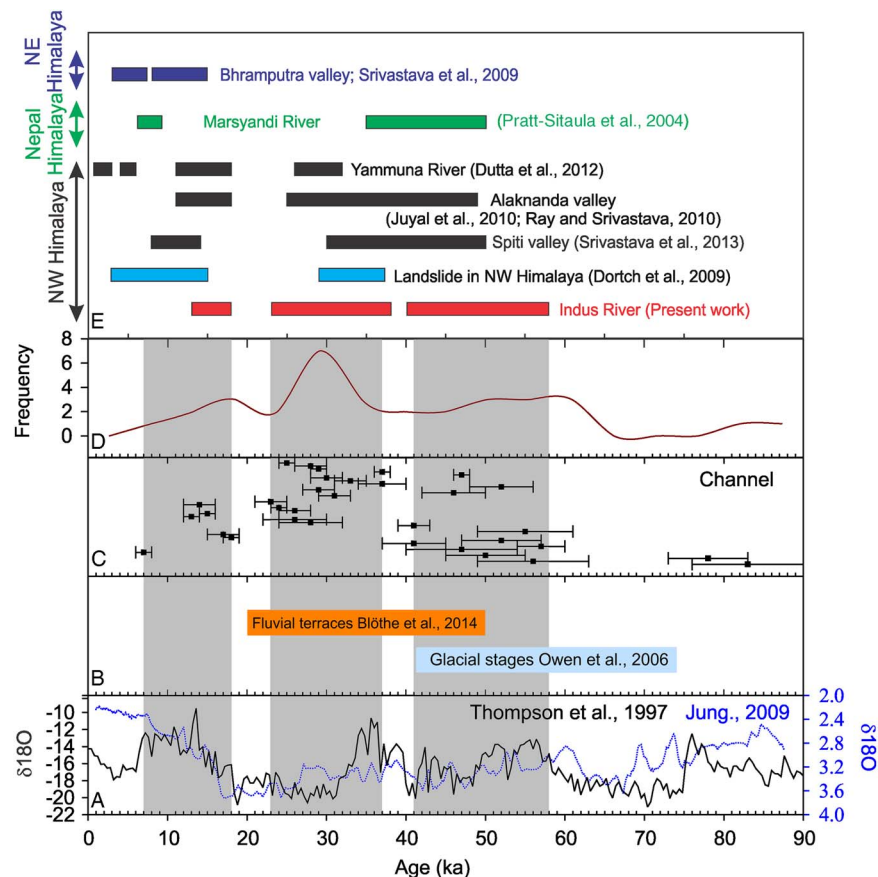
Figure 9. (color online) Valley aggradation in the Indus River and paleoclimate record. (A) Climate record from the Guliya Ice Core (after Thompson et al., 1997) and Arabian Sea NIOP905 87KYr Benthic Stable Isotope Data (Jung et al., 2010). (B) Paleoglacial record of Ladakh. (C) Age distribution of the channel bound and outwash fan sediment. (D) Frequency distribution of all the ages. (E) Major phases of aggradation shown by prominent river in northwest (NW), Nepal, and northeast (NE) Himalaya. Note that widespread aggradation of channel took place during the Marine Oxygen Isotope Stages (MIS) 1 and MIS 3, and sedimentation of alluvial fans in Ladakh took place during the deglaciation of MIS 3 only.

vegetation cover that reduced the sediment to water ratio, incision occurred. This in general was true for all the rivers along the Himalayan arc (Ray and Srivastava, 2010; Scherler et al., 2015; Sinclair et al., 2017).

Channel gradient indices, strath terrace formation, and incision rates

Ideally, the channel gradient indices exhibit higher values for regions with molasse (sandstone and shale) and lower values for regions of granitic batholith (Troiani et al., 2014). Our results, however, do not show this trend (Fig. 2). K_s values show a similar trend (i.e., higher for regions with granite and lower for regions with molasse) (Munack et al., 2014). These suggest that for the Indus River the channel steepness was controlled by tectonic uplifts and the bedrock erodibility played a subordinate role. Channel steepness for non-glaciated catchments bordering the Indus River and in the southeast (SE) Tibetan plateau front provides a similar inference (Kirby et al., 2003; Sinclair et al., 2017).

In segment 2, a steep channel gradient and high SL index indicate the river's adjustment to active tectonics and uplift in

its headwater region. Similar observations accrue from SE Tibet, where longitudinal river profiles were steep and adjusted to differential uplift between Tibet and its surrounding (Kirby et al., 2003). Varied evidence based on sedimentology and geomorphology has suggested recent uplifts in southern Tibet (Liu, 1981; Li and Zhou, 2001), and these lead to vertical incision. [10]Be-based modern erosion rates above and below the knick point at Mahe indicate strong headward erosion and incision by the Indus (Munack et al., 2014). This also suggests that the incision in segment 2 was partly driven by the elevation of the Tibetan plateau.

OSL chronology in segment 3 indicates that the alluvial fan aggradation and river valley filling occurred during 47–29 ka. Therefore, excess sediment delivery from the Zanskar ranges that were additionally pushing the river northward led to a lower SL index. The Stok, Upshi-Bazgo, and Choksti Thrusts located along and south of the Indus River, respectively, were active, and tectonic activity along these thrusts aided by the high relief of the Zanskar ranges led to excess sediment supply. [10]Be-derived denudation rates of 69.8 mm/ka in Zanskar bound rivers are high as compared with 29 mm/ka of those draining the batholith suggesting that

the Indus Molasse sequence is actively deforming and rising (Searle et al., 1990; Sinclair and Jaffey, 2001; Munack et al., 2014; Sinclair et al., 2017). High sediment supply and aggradation in this segment helped lower the gradient and the SL index of the channel.

In segment 4, chronologies of the alluvial cover preserved over the strath terraces indicate incision rates of ~0.8–3.0 mm/a. The height and chronology of strath terraces indicated two levels of former riverbed profiles of the Indus (Fig. 10A and B). The upper profile is at an average elevation of 134 ± 24 m arl and has an OSL age of 62 ± 16 ka, and these imply an average incision rate of 2.2 ± 0.9 mm/a. The lower profile, at 45 ± 5 m arl with an OSL age of 44 ± 8 ka (Fig. 8D), implies an erosion rate of 1.0 ± 0.3 mm/a. Interpolation of these profiles upstream in the present river profile indicates that: (1) the lower profile truncates into the fill sequences preserved in segment 3 (Leh valley) as both bear similar ages; and (2) the upper profile is older, and sediment of equivalent age might be present in the subsurface in segment 3 and upstream. The sequences above the present riverbed, upstream from Nimu, do not have any sediment that is equal to, or older in age than 62 ± 16 ka. This suggests that a divergence of both lower and upper profiles occurred because of a fall in the base level in the downstream region (Pazzaglia et al., 1998; Crosby and Whipple, 2006; Wobus et al., 2006). Bedrock incision rates deduced in this study and rock uplift rates in the region may not correlate. Investigations in Marsyandi River, Nepal, show that while the uplift continues, the alluvial fill protects the riverbed from incision, and later after the removal of the fill, the river incises at rates faster than the mean (Pratt-Sitaula et al., 2004). We consider this to be the same in the study area.

Bedrock incision rates and base level fall at Nanga Parbat–Harmosh Massif (NPHM)

In NPHM of the western syntaxes, two sets of strath terraces along the Indus are dated using terrestrial cosmogenic nuclides to ~7 ka and between 67 and 27 ka (Burbank et al., 1996; Leland et al., 1998) yielding bedrock incision rates of 9–12 mm/a during the Holocene and 1–6 mm/a during pre–last glacial maximum. Modern incision rates of the Indus in NPHM are ~12 mm/a, and these reduce to 3–6 mm/a ~50 km upstream at Skardu. Postglacial incision rates of Shigar, a tributary of Braldu River that flows into the Indus near Skardu, are 2–29 mm/a (Seong et al., 2008). Therefore, the present study and the published data suggest that the incision rates along the Indus River increase sharply from 0.8–3.0 to ~12 mm/a as it flows from Nimu to NPHM in the western syntaxes (Fig. 10C). [10]Be-based bulk erosion rates along the Indus also show an increase in NW direction that reaches its maxima at the western syntaxes (Garzanti et al., 2005; Van Der Beek et al., 2009; Ali and de Boer, 2010; Munack et al., 2014). This suggests that erosion and downcutting by the Indus River were controlled by the base level fall at NPHM.

Increase in the channel slope and bedrock incision in the downstream reaches can produce a knick point that moves upstream and that in the long term can induce incision as far as 300 km upstream (Gardner, 1983). In the case of the Indus River, the presence of a wide basin at Skardu that lies between NPHM and Nimu can possibly hinder the upstream movement of the knick point. However, in the Skardu basin and NPHM, the channel gradient are 3.3 and 10.8 m/km, respectively. These are higher than that 1.8 m/km at Leh. These, therefore, indicate progressive steepening of the river valley in the downstream reaches. Structural and geomorphic analysis suggests that incision and aggradation in the Skardu basin itself was controlled by the far-field effect of rapid uplift in the NPHM zone and north–south compression along the Himalayan arc (Cronin, 1989). Thus, incision rates determined by earlier studies and those in the present study provide insight into the response of tectonics and the far-field effects of rapid uplift in the NPHM of the western syntaxes and formation of strath terraces in segment 4.

Distribution of strath terrace T-2 along the longitudinal profile shows initiation of the knick points in the most downstream part at ~83 ka (Skyurbuchan Downstream section; Fig. 8D) and that moved in the upstream, such that terrace at the same level yields younger ages of ~50 ka. The age of ~78 ka for the strath terrace, T-2, at Nurla section is an exception and still needs a proper explanation through structural mapping of the area.

Formation of strath terraces in segment 4, between Nimu and upstream of Dah, can be understood in two different scenarios as well. The first scenario considers that in segment 4 river flows through the Indus Molasse sequence, which is deformed and comprises several north-verging thrusts like the Choksti, Stok, and Upshi-Bazgo Thrusts. Chronological data on strath terraces indicate that these thrusts are neotectonically active and the river has responded to uplift along these thrusts. OSL ages of 42 ka for fluvial terraces and the geomorphic setting around Leh indicate neotectonic deformation of the Indus Molasse along the Stok Thrust and that a shortening of ~10 m controlled the landscape development (Sinclair et al., 2017). Further evidence of tectonic movement accrues from the following: (1) steepness index in the hanging wall of the Stok Thrust (Sinclair et al., 2017), the basin morphometry, and hypsometric indices of tributaries draining into the Indus and Shyok Rivers between Leh and Khalsi (zone B of Jamieson et al., 2004); (2) increasing channel sinuosity with river downcutting in the form of entrenched meanders at Nimu (Gardner, 1975; Schumm et al., 1987; Rogers et al., 2002); and (3) records of seismites along the Indus River at Spituk, Saspol, and Lamayuru, as well as other surrounding areas that point toward past seismic activity in the region (Bagati et al., 1996; Singh and Jain, 2007; Phartiyal and Sharma, 2009).

An alternative scenario is where fills overlying the strath terraces in the Nimu–Dah segment and those in the Leh valley are coeval and represent a single phase of valley alluviation in the Indus as suggested earlier (Blöthe et al. 2014). Excess sediment brought down by the Zanskar River potentially choked the gorge and dammed the Indus near Spituk, and a lake formed that existed for at least 100 ka (Blöthe et al. 2014). This suggests that the ~35 m Spituk lake sequence took >100 ka to aggrade; implying an average sedimentation rate of 0.35 mm/yr, which is not realistic. The varve and
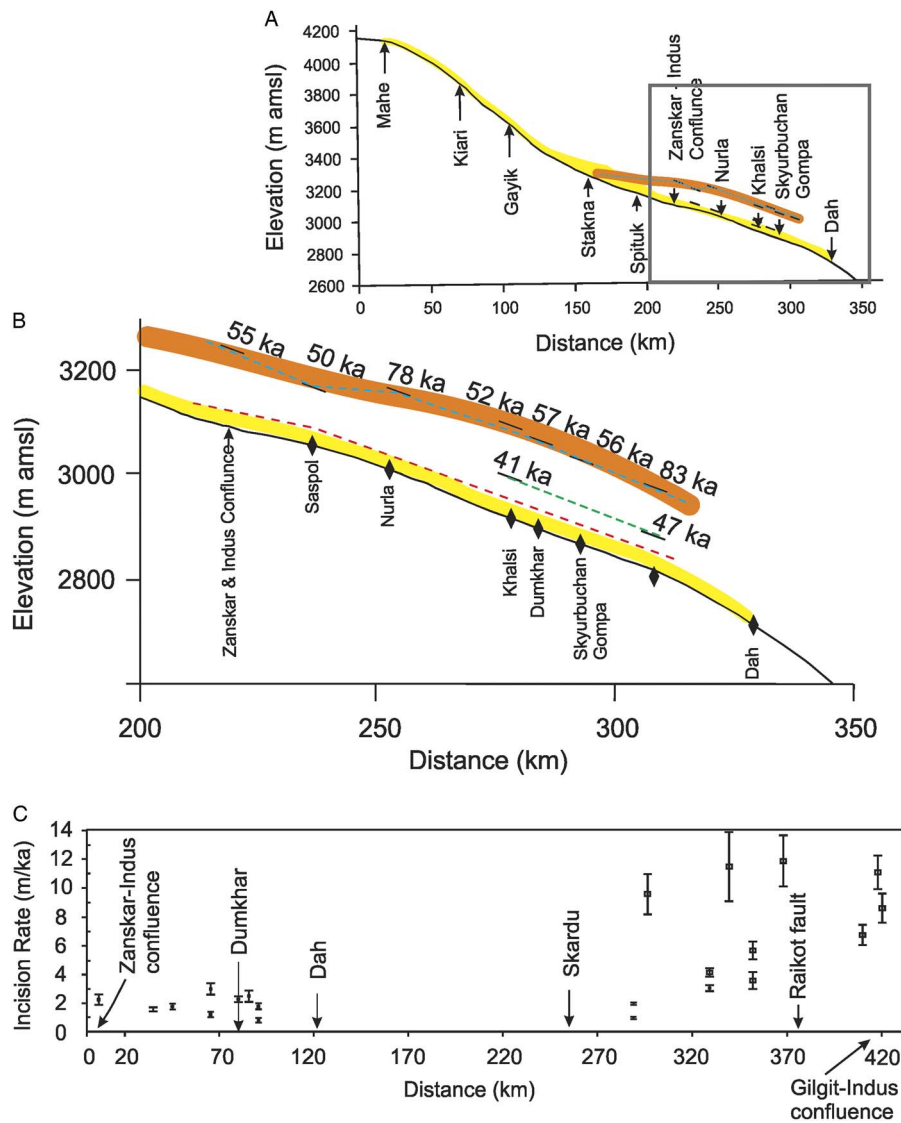
Figure 10. (color online) (A) Longitudinal river profile of the Indus River with strath terraces. Note the downstream divergent nature of the strath profile. (B) Longitudinal profile of the Indus showing reconstruction of two levels of paleoriverbeds and ages of the strath terraces. (C) Comparison of bedrock incision rates in the Nanga Parbat–Harmosh Massif region of the western syntaxes (after Leland et al., 1998) and the incision rates deduced in this study. Note the systematic downstream increase in the incision rates. m amsl, meters above mean sea level.

sedimentary rythmites in the Spituk sequence that are supposed to be annual sedimentary layers are less than a centimeter in thickness indicating a much higher sedimentation rate (3–4 mm/yr; Nag et al., 2016). The chronological data published from the paleolake sequences from across the Himalaya also seem to suggest much higher sedimentation rates (Fort, 2000; Korup et al., 2006; Phartiyal et al., 2009; Anoop et al., 2013; Srivastava et al., 2013; Nag and Phartiya, 2015).

CONCLUSION

The upper Indus River that we studied exhibits a complex interaction among the channel aggradation, progradation of alluvial fans, landslides, and high sediment supply from

tributaries that caused local damming and transient filling of the river. Several possible explanations for valley filling, lake formation, and strath chronology in the Indus River exist, but the more preferred explanation is the climate-driven valley aggradation and incision attributable to tectonics and the fall in NPHM base level.

The valley filling was controlled by bar aggradation associated with channel and alluvial fan progradation. Aggradation occurred in three pulses at ~52, ~28, and ~16 ka; aggradation on alluvial fans took place from ~47 to 29 ka. These were during the well-documented periods of strengthened SW monsoon conditions.

Strath terraces in the Nimu–Dah segment suggest two past levels of the Indus. The upper profile at an elevation of 134 ± 24 m arl has an age of 62 ± 16 ka yielding an average

erosion rate of 2.2 ± 0.9 mm/a. The lower profile at 45 ± 5 m arl has an age of 44 ± 8 ka and an average erosion rate of 1.0 ± 0.3 mm/a.

Incision rates from NPHM suggest that the strath development in segment 4 was because of a far-field effect of uplift and rapid incision in the western syntaxes.

Active tectonic deformation of the Indus Molasse during the past ~50 ka led to the incision of the river and influenced the sedimentary architecture of fills.

Results of our study pose an important question as to what degree do tectonics influence landscape evolution along the upper Indus valley.

ACKNOWLEDGMENTS

SUPPLEMENTARY MATERIAL

To view supplementary material for this article, please visit https://doi.org/qua.2017.19

REFERENCES

Aitken, M.J., 1998. *An Introduction to Optical Dating*. Academic Press, London.

Ali, K.F., de Boer, D.H., 2010. Spatially distributed erosion and sediment yield modelling in the upper Indus River basin. *Water Resources Research* 46, W08504. http://dx.doi.org/10.1029/2009WR008762.

Ali, S.N., Juyal, N., 2013. Chronology of late quaternary glaciations in Indian Himalaya: a critical review. *Journal of the Geological Society of India* 82, 628–638.

Anders, A.M., Roe, G.H., Hallet, B., Montgomery, D.R., Finnegan, N.J., Putkonen, J., 2006. Spatial patterns of precipitation and topography in the Himalaya. *Geological Society of America, Special Papers* 398, 39–53.

Anoop, A., Prasad, S., Krishnan, R., Naumann, R., Dulski, P., 2013. Intensified monsoon and spatiotemporal changes in precipitation patterns in the NW Himalaya during the early-mid Holocene. *Quaternary International* 313, 74–84.

Bagati, T.N., Mazari, R.K., Rajagopalan, G., 1996. Palaeotectonic implication of Lamayuru Lake (Ladakh). *Current Science* 71, 479–482.

Blöthe, J.H., Munack, H., Korup, O., Fülling, A., Garzanti, E., Resentini, A., Kubik, P.W., 2014. Late Quaternary valley infill and dissection in the Indus River, western Tibetan Plateau margin. *Quaternary Science Reviews* 94, 102–119.

Blum, M.D., Törnqvist, T.E., 2000. Fluvial responses to climate and sea-level change: a review and look forward. *Sedimentology* 47, 2–48.

Bookhagen, B., Burbank, D.W., 2010. Toward a complete Himalayan hydrological budget: spatiotemporal distribution of snowmelt and rainfall and their impact on river discharge. *Journal of Geophysical Research: Earth Surface* 115, F03019. http://dx.doi.org/10.1029/2009JF001426.

Bookhagen, B., Thiede, R.C., Strecker, M.R., 2005. Late Quaternary intensified monsoon phases control landscape evolution in the northwest Himalaya. *Geology* 33, 149–152.

Brookfield, M.E., Andrews-Speed, C.P., 1984. Sedimentology, petrography and tectonic significance of the shelf, flysch and molasse clastic deposits across the Indus Suture Zone, Ladakh, NW India. *Sedimentary Geology* 40, 249–286.

Bull, W.B., 1990. Stream-terrace genesis: implications for soil development. *Geomorphology* 3, 351–367.

Burbank, D.W., Leland, J., Fielding, E., Anderson, R., Brozovic, N., Reid, M., Duncan, C., 1996. Bedrock incision, rock uplift and threshold hillslopes in the northwestern Himalayas. *Nature* 379, 505–510.

Clarke, M.L., 1996. IRSL dating of sands: bleaching characteristics at deposition inferred from the use of single aliquots. *Radiation Measurements* 26, 611–620.

Clift, P.D., Giosan, L., 2014. Sediment fluxes and buffering in the post-glacial Indus Basin. *Basin Research* 26, 369–386.

Colls, A.E., Stokes, S., Blum, M.D., Straffin, E., 2001. Age limits on the Late Quaternary evolution of the upper Loire River. *Quaternary Science Reviews* 20, 743–750.

Cronin, V.S., 1989. Structural setting of the Skardu intermontane basin, Karakorum Himalaya, Pakistan. Geological Society of America, Special Papers 232, 183–202.

Crosby, B.T., Whipple, K.X., 2006. Knickpoint initiation and distribution within fluvial networks: 236 waterfalls in the Waipaoa River, North Island, New Zealand. *Geomorphology* 82, 16–38.

Demske, D., Tarasov, P.E., Wünnemann, B., Riedel, F., 2009. Late glacial and Holocene vegetation, Indian monsoon and westerly circulation in the Trans-Himalaya recorded in the lacustrine pollen sequence from Tso Kar, Ladakh, NW India. *Palaeogeography, Palaeoclimatology, Palaeoecology* 279, 172–185.

Derbyshire, E., Owen, L.A., 1997. Quaternary glacial history of the Karakoram Mountains and Northwest Himalayas: a review. *Quaternary International* 38, 85–102.

Devrani, R., Singh, V., 2014. Evolution of valley-fill terraces in the Alaknanda Valley, NW Himalaya: its implication on river response studies. *Geomorphology* 227, 112–122.

Dortch, J.M., Owen, L.A., Caffee, M.W., 2013. Timing and climatic drivers for glaciation across semi-arid western Himalayan Tibetan orogen. *Quaternary Science Reviews* 78, 188–208.

Dortch, J.M., Owen, L.A., Dietsch, C., Caffee, M.W., Bovard, K., 2011a. Episodic fluvial incision of rivers and rock uplift in the Himalaya and Trans-Himalaya. *Journal of the Geological Society* 168, 783–804.

Dortch, J.M., Owen, L.A., Haneberg, W.C., Caffee, M.W., Dietsch, C., Kamp, U., 2009. Nature and timing of large landslides in the Himalaya and Trans Himalaya of northern India. *Quaternary Science Reviews* 28, 1037–1054.

Dortch, J.M., Owen, L.A., Schoenbohm, L.M., Caffee, M.W., 2011b. Asymmetrical erosion and morphological development of the central Ladakh Range, northern India. *Geomorphology* 135, 167–180.

Drew, F., 1873. Alluvial and lacustrine deposits and glacial records of the Upper-Indus Basin. *Quarterly Journal of the Geological Society* 29, 441–471.

Dutta, S., Suresh, N., Kumar, R., 2012. Climatically controlled Late Quaternary terrace staircase development in the fold-and-thrust belt of the Sub Himalaya. *Palaeogeography, Palaeoclimatology, Palaeoecology* 356, 16–26.

Fang, J.Q., 1991. Lake evolution during the past 30,000 years in China, and its implications for environmental change. *Quaternary Research* 36, 37–60.

Fort, M., 2000. Glaciers and mass wasting processes: their influence on the shaping of the Kali Gandaki valley (higher Himalaya of Nepal). *Quaternary International* 65, 101–119.

Galbraith, R.F., Roberts, R.G., Laslett, G.M., Yoshida, H., Olley, J. M., 1999. Optical dating of single and multiple grains of quartz from Jinmium rock shelter, northern Australia: part I, experimental design and statistical models. *Archaeometry* 41, 339–364.

Gardner, T.W., 1975. The history of part of the Colorado River and its tributaries: an experimental study. *Four Corners Geological Society Guidebook* 8, 87–95.

Gardner, T.W., 1983. Experimental study of knickpoint and longitudinal profile evolution in cohesive, homogeneous material. *Geological Society of America Bulletin* 94, 664–672.

Garzanti, E., Vezzoli, G., Andó, S., Paparella, P., Clift, P., 2005. Petrology of Indus River sands: a key to interpret erosion history of the Western Himalayan syntaxis. *Earth and Planetary Science Letters* 229, 287–302.

Goodbred, S.L., 2003. Response of the Ganges dispersal system to climate change: a source-to-sink view since the last interstade. *Sedimentary Geology* 162, 83–104.

Hack, J.T., 1973. Stream-profile analysis and stream-gradient index. *Journal of Research of the U.S. Geological Survey* 1, 421–429.

Hancock, G.S., Anderson, R.S., 2002. Numerical modeling of fluvial strath-terrace formation in response to oscillating climate. *Geological Society of America Bulletin* 114, 1131–1142.

Henderson, A.L., Najman, Y., Parrish, R., BouDagher-Fadel, M., Barford, D., Garzanti, E., Andò, S., 2010. Geology of the Cenozoic Indus Basin sedimentary rocks: paleoenvironmental interpretation of sedimentation from the western Himalaya during the early phases of India-Eurasia collision. *Tectonics* 29, TC6015. http://dx.doi.org/10.1029/2009TC002651.

Henderson, A.L., Najman, Y., Parrish, R., Mark, D.F., Foster, G.L., 2011. Constraints to the timing of India–Eurasia collision: a re-evaluation of evidence from the Indus Basin sedimentary rocks of the Indus–Tsangpo Suture Zone, Ladakh, India. *Earth-Science Reviews* 106, 265–292.

Hobley, D.E., Sinclair, H.D., Mudd, S.M., 2012. Reconstruction of a major storm event from its geomorphic signature: the Ladakh floods, 6 August 2010. *Geology* 40, 483–486.

Howard, J.L., 1993. The statistics of counting clasts in rudites: a review, with examples from the upper Palaeogene of southern California, USA. *Sedimentology* 40, 157–174.

Jade, S., Rao, H.J.R., Vijayan, M.S.M., Gaur, V.K., Bhatt, B.C., Kumar, K., Jaganathan, S., Ananda, M.B., Kumar, P.D., 2011. GPS-derived deformation rates in northwestern Himalaya and Ladakh. *International Journal of Earth Sciences* 100, 1293–1301.

Jain, M., Murray, A.S., Bøtter-Jensen, L., Wintle, A.G., 2005. A single-aliquot regenerative-dose method based on IR bleaching of the fast OSL component in quartz. *Radiation Measurements* 39, 309–318.

Jamieson, S.S.R., Sinclair, H.D., Kirstein, L.A., Purves, R.S., 2004. Tectonic forcing of longitudinal valleys in the Himalaya: morphological analysis of the Ladakh Batholith, North India. *Geomorphology* 58, 49–65.

Jung, S.J.A., Kroon, D., Ganssen, G., Peeters, F., Ganeshram, R., 2009. Enhanced Arabian Sea intermediate water flow during glacial North Atlantic cold phases. *Earth and Planetary Science Letters* 280, 220–228.

Jung, S.J.A., Kroon, D., Ganssen, G., Peeters, F., Ganeshram, R., 2010. Arabian Sea NIOP905 87KYr Benthic Stable Isotope Data. IGBP PAGES/World Data Center for Paleoclimatology Data Contribution Series No. 2010-034. National Oceanic and Atmospheric Administration/National Climatic Data Center Paleoclimatology Program, Boulder, CO.

Juyal, N., Pant, R.K., Basavaiah, N., Bhushan, R., Jain, M., Saini, N. K., Yadava, M.G., Singhvi, A.K., 2009. Reconstruction of Last Glacial to early Holocene monsoon variability from relict lake sediments of the Higher Central Himalaya, Uttrakhand, India. *Journal of Asian Earth Sciences* 34, 437–449.

Juyal, N., Sundriyal, Y.P., Rana, N., Chaudhary, S., Singhvi, A.K., 2010. Late Quaternary fluvial aggradation and incision in the monsoon-dominated Alaknanda valley, Central Himalaya, Uttrakhand, India. *Journal of Quaternary Science* 25, 1293–1304.

Kirby, E., Whipple, K.X., Tang, W., Chen, Z., 2003. Distribution of active rock uplift along the eastern margin of the Tibetan Plateau: inferences from bedrock channel longitudinal profiles. *Journal of Geophysical Research: Solid Earth* 108, 2217.

Korup, O., Strom, A.L., Weidinger, J.T., 2006. Fluvial response to large rock-slope failures: examples from the Himalayas, the Tien Shan, and the Southern Alps in New Zealand. *Geomorphology* 78, 3–21.

Kumar, A., Srivastava, P., Meena, N.K., 2016. Late Pleistocene aeolian activity in the cold desert of Ladakh: a record from sand ramps. Quaternary International (in press). http://dx.doi.org/10.1016/j.quaint.2016.04.006.

Lang, T.J., Barros, A.P., 2004. Winter storms in the central Himalayas. *Journal of the Meteorological Society of Japan* 82, 829–844.

Lavé, J., Avouac, J.P., 2000. Active folding of fluvial terraces across the Siwalik Hills, Himalayas of central Nepal. *Journal of Geophysical Research: Solid Earth* 105, 5735–5770.

Lavé, J., Avouac, J.P., 2001. Fluvial incision and tectonic uplift across the Himalayas of central Nepal. *Journal of Geophysical Research: Solid Earth* 106, 26561–26591.

Leland, J., Reid, M.R., Burbank, D.W., Finkel, R., Cafee, M., 1998. Incision and differential bedrock uplift along the Indus River near Nanga Parbat, Pakistan Himalaya, from [10]Be and [26]Al exposure age dating of bedrock straths. *Earth and Planetary Science Letters* 154, 93–107.

Li, J., Zhou, Y., 2001. Palaeovegetation type analysis of the late Pliocene in Zanda basin of Tibet. *Journal of Palaeogeography* 14, 52–58.

Liu, D. (Ed.), 1981. *Geological and Ecological Studies of Qinghai-Xizang Plateau. Vol. 1, Geologic, Geological History and Origin of Qinghai-Xizang Plateau*. Science Press, Beijing.

Miall, A.D., 1996. *The Geology of Fluvial Deposits*. Springer, Berlin.

Morell, K.D., Sandiford, M., Rajendran, C.P., Rajendran, K., Alimanovic, A., Fink, D., Sanwal, J., 2015. Geomorphology reveals active décollement geometry in the central Himalayan seismic gap. *Lithosphere* 7, 247–256.

Munack, H., Korup, O., Resentini, A., Limonta, M., Garzanti, E., Blöthe, J.H., Scherler, D., Wittmann, H., Kubik, P.W., 2014. Postglacial denudation of western Tibetan Plateau margin outpaced by long-term exhumation. *Geological Society of America Bulletin* 126, 1580–1594.

Murray, A.S., Wintle, A.G., 2000. Luminescence dating of quartz using an improved single aliquot regenerative-dose protocol. *Radiation Measurements* 32, 57–73.

Nag, D., Phartiyal, B., 2015. Climatic variations and geomorphology of the Indus River valley, between Nimo and Batalik, Ladakh (NW Trans Himalayas) during Late Quaternary. *Quaternary International* 371, 87–101.

Nag, D., Phartiyal, B., Singh, D.S., 2016. Sedimentary characteristics of palaeolake deposits along the Indus River valley, Ladakh, Trans-Himalaya: implications for the depositional environment. *Sedimentology* 63, 1765–1785.

Owen, L.A., Bailey, R.M., Rhodes, E.J., Mitchell, W.A., Coxon, P., 1997. Style and timing of glaciation in the Lahul Himalaya, northern India: a framework for reconstructing late Quaternary palaeoclimatic change in the western Himalayas. *Journal of Quaternary Science* 12, 83–109.

Owen, L.A., Benn, D.I., 2005. Equilibrium-line altitudes of the Last Glacial Maximum for the Himalaya and Tibet: an assessment and evaluation of results. *Quaternary International* 138, 55–78.

Owen, L.A., Caffee, M.W., Bovard, K.R., Finkel, R.C., Sharma, M.C., 2006a. Terrestrial cosmogenic nuclide surface exposure dating of the oldest glacial successions in the Himalayan orogen: Ladakh Range, northern India. *Geological Society of America Bulletin* 118, 383–392.

Owen, L.A., Caffee, M.W., Finkel, R.C., Seong, B.Y., 2008. Quaternary glaciations of the Himalayan Tibetan orogen. *Journal of Quaternary Science* 23, 513–532.

Owen, L.A., Dortch, J.M., 2014. Nature and timing of Quaternary glaciation in the Himalayan Tibetan orogen. *Quaternary Science Reviews* 88, 14–54.

Owen, L.A., Finkel, R.C., Barnard, P.L., Haizhou, M., Asahi, K., Caffee, M.W., Derbyshire, E., 2005. Climatic and topographic controls on the style and timing of late Quaternary glaciation throughout Tibet and the Himalaya defined by ^{10}Be cosmogenic radionuclide surface exposure dating. *Quaternary Science Reviews* 24, 1391–1411.

Owen, L.A., Finkel, R.C., Haizhou, M., Barnard, P.L., 2006b. Late Quaternary landscape evolution in the Kunlun Mountains and Qaidam Basin, Northern Tibet: a framework for examining the links between glaciation, lake level changes and alluvial fan formation. *Quaternary International* 154, 73–86.

Owen, L.A., Gualtieri, L., Finkel, R.C., Caffee, M.W., Benn, D.I., Sharma, M.C., 2001. Cosmogenic radionuclide dating of glacial landforms in the Lahul Himalaya, northern India: defining the timing of Late Quaternary glaciation. *Journal of Quaternary Science* 16, 555–563.

Orr, E.N., Owen, L.A., Murari, M.K., Saha, S., Caffee, M.W., 2017. The timing and extent of Quaternary glaciation of Stok, northern Zanskar Range, Transhimalaya, of northern India. *Geomorphology* 284, 142–155.

Pant, R.K., Phadtare, N.R., Chamyal, L.S., Juyal, N., 2005. Quaternary deposits in Ladakh and Karakoram Himalaya: a treasure trove of the palaeoclimate records. *Current Science* 88, 1789–1798.

Pazzaglia, F.J., Gardner, T.W., Merritts, D.J., 1998. Bedrock fluvial incision and longitudinal profile development over geologic time scales determined by fluvial terraces. In: Tinkler, K.J., Wohl, E.E. (Eds.), *Rivers over Rock: Fluvial Processes in Bedrock Channels*. American Geophysical Union, Washington, DC, pp. 207–235.

Phartiyal, B., Sharma, A., 2009. Soft-sediment deformation structures in the Late Quaternary sediments of Ladakh: evidence for multiple phases of seismic tremors in the north western Himalayan region. *Journal of Asian Earth Sciences* 34, 761–770.

Phartiyal, B., Sharma, A., Kothari, G.C., 2013. Existence of Late Quaternary and Holocene lakes along the River Indus in Ladakh region of Trans Himalaya, NW India: implications to climate and tectonics. *Chinese Science Bulletin* 58, 1–14.

Phartiyal, B., Sharma, A., Srivastava, P., Ray, Y., 2009. Chronology of relict lake deposits in the Spiti River, NW Tran Himalaya: implications to Late Pleistocene-Holocene climate-tectonic perturbations. *Geomorphology* 108, 264–272.

Phartiyal, B., Sharma, A., Upadhyay, R., Sinha, A.K., 2005. Quaternary geology, tectonics and distribution of palaeo-and present fluvio/glacio lacustrine deposits in Ladakh, NW Indian Himalaya—a study based on field observations. *Geomorphology* 65, 241–256.

Pratt-Sitaula, B., Burbank, D.W., Heimsath, A., Ojha, T., 2004. Landscape disequilibrium on 1000–10,000 year scales Marsyandi River, Nepal, central Himalaya. *Geomorphology* 58, 223–241.

Prell, W.L., Kutzbach, J.E., 1987. Monsoon variability over the past 150,000 years. *Journal of Geophysical Research: Atmospheres* 92, 8411–8425.

Prescott, J.R., Hutton, J.T., 1994. Cosmic ray contributions to dose rates for luminescence and ESR dating: large depths and long-term time variations. *Radiation Measurements* 23, 497–500.

Rawat, S., Gupta, A.K., Sangode, S.J., Srivastava, P., Nainwal, H.C., 2015a. Late Pleistocene–Holocene vegetation and Indian summer monsoon record from the Lahaul, Northwest Himalaya, India. *Quaternary Science Reviews* 114, 167–181.

Rawat, S., Gupta, A.K., Srivastava, P., Sangode, S.J., Nainwal, H.C., 2015b. A 13,000 year record of environmental magnetic variations in the lake and peat deposits from the Chandra valley, Lahaul: implications to Holocene monsoonal variability in the NW Himalaya. *Palaeogeography, Palaeoclimatology, Palaeoecology* 440, 116–127.

Ray, Y., Srivastava, P., 2010. Widespread aggradation in the mountainous catchment of the Alaknanda Ganga River System: timescales and implications to hinterland foreland relationships. *Quaternary Science Reviews* 29, 2238–2260.

Rogers, R.D., Kárason, H., van der Hilst, R.D., 2002. Epeirogenic uplift above a detached slab in northern Central America. *Geology* 30, 1031–1034.

Saha, S., Sharma, M.C., Murari, M.K., Owen, L.A., Caffee, M.W., 2016. Geomorphology, sedimentology and minimum exposure ages of streamlined subglacial landforms in the NW Himalaya, India. *Boreas* 45, 284–303.

Sangode, S.J., Phadtare, N.R., Meshram, D.C., Rawat, S., Suresh, N., 2011. A record of lake outburst in the Indus valley of Ladakh Himalaya, India. *Current Science* 100, 1712–1718.

Sangode, S.J., Rawat, S., Meshram, D.C., Phadtare, N.R., Suresh, N., 2013. Integrated mineral magnetic and lithologic studies to delineate dynamic modes of depositional conditions in the Leh valley basin, Ladakh Himalaya, India. *Journal of the Geological Society of India* 82, 107–120.

Sant, D.A., Wadhawan, S.K., Ganjoo, R.K., Basavaiah, N., Sukumaran, P., Bhattacharya, S., 2011a. Linkage of paraglacial processes from last glacial to recent inferred from Spituk sequence, Leh valley, Ladakh Himalaya. *Journal of the Geological Society of India* 78, 147–156.

Sant, D.A., Wadhawan, S.K., Ganjoo, R.K., Basavaiah, N., Sukumaran, P., Bhattacharya, S., 2011b. Morphostratigraphy and palaeoclimate appraisal of the Leh valley, Ladakh Himalayas, India. *Journal of the Geological Society of India* 77, 499–510.

Scherler, D., Bookhagen, B., Wulf, H., Preusser, F., Strecker, M.R., 2015. Increased late Pleistocene erosion rates during fluvial aggradation in the Garhwal Himalaya, northern India. *Earth and Planetary Science Letters* 428, 255–266.

Schumm, S., Mosley, P., Weaver, W., 1987. *Experimental Fluvial Geomorphology*. John Wiley and Sons, New York.

Searle, M.P., 1986. Structural evolution and sequence of thrusting in the High Himalayan, Tibetan-Tethys and Indus suture zones of Zanskar and Ladakh, Western Himalaya. *Journal of Structural Geology* 8, 923–936.

Searle, M.P., Pickering, K., Cooper, D., 1990. Restoration and evolution of the intermontane Indus molasse basin, Ladakh Himalaya, India. *Tectonophysics* 174, 301–314.

Seong, Y.B., Owen, L.A., Bishop, M.P., Bush, A., Clendon, P., Copland, L., Finkel, R.C., Kamp, U., Shroder, J.F., 2008. Rates of fluvial bedrock incision within an actively uplifting orogen: Central Karakoram Mountains, northern Pakistan. *Geomorphology* 97, 274–286.

Sharma, S., Bartarya, S.K., Marh, B.S., 2016a. Post-glacial landform evolution in the middle Satluj River valley, India: implications towards understanding the climate tectonic interactions. *Journal of Earth System Science* 125, 539–558.

Sharma, S., Chand, P., Bisht, P., Shukla, A.D., Bartarya, S.K., Sundriyal, Y.P., Juyal, N., 2016b. Factors responsible for driving the glaciation in the Sarchu Plain, eastern Zanskar Himalaya, during the late Quaternary. *Journal of Quaternary Science* 31, 495–511.

Shi, Y., Yu, G., Liu, X., Li, B., Yao, T., 2001. Reconstruction of the 30–40 ka BP enhanced Indian monsoon climate based on geological records from the Tibetan Plateau. *Palaeogeography, Palaeoclimatology, Palaeoecology* 169, 69–83.

Shukla, U.K., 2009. Sedimentation model of gravel-dominated alluvial piedmont fan, Ganga Plain, India. *International Journal of Earth Sciences* 98, 443–459.

Sinclair, H.D., Jaffey, N., 2001. Sedimentology of the Indus Group, Ladakh, northern India: implications for the timing of initiation of the palaeo-Indus River. *Journal of the Geological Society* 158, 151–162.

Sinclair, H.D., Mudd, S.M., Dingle, E., Hobley, D.E.J., Robinson, R., Walcott, R., 2017. Squeezing river catchments through tectonics: shortening and erosion across the Indus Valley, NW Himalaya. *Geological Society of America Bulletin* 129, 203–217.

Singh, I.B., Sahni, A., Jain, A.K., Upadhyay, R., Parcha, S.K., Parmar, V., Agarwal, K.K., *et al*. 2015. Post-collision sedimentation in the Indus Basin (Ladakh, India): implications for the evolution of the northern margin of the Indian plate. *Journal of the Palaeontological Society of India* 60, 97–146.

Singh, S., Jain, A.K., 2007. Liquefaction and fluidization of lacustrine deposits from Lahaul-Spiti and Ladakh Himalaya: geological evidences of paleoseismicity along active fault zone. *Sedimentary Geology* 196, 47–57.

Srivastava, P., Bhakuni, S.S., Luirei, K., Misra, D.K., 2009. Morpho-sedimentary records from the Brahmaputra River exit, NE Himalaya: climate-tectonic interplay during Late Pleistocene-Holocene. *Journal of Quaternary Science* 24, 175–188.

Srivastava, P., Brook, G.A., Marais, E., Morthekai, P., Singhvi, A.K., 2006. Depositional environment and OSL chronology of the Homeb silt deposits, Kuiseb River, Namibia. *Quaternary Research* 65, 478–491.

Srivastava, P., Misra, D.K., 2008. Morpho-sedimentary records of active tectonics at the Kameng River exit, NE Himalaya. *Geomorphology* 96, 187–198.

Srivastava, P., Ray, Y., Phartiyal, B., Sharma, A., 2013. Late Pleistocene-Holocene morphosedimentary architecture, Spiti River, arid higher Himalaya. *International Journal of Earth Sciences* 102, 1967–1984.

Srivastava, P., Tripathi, J.K., Islam, R., Jaiswal, M.K., 2008. Fashion and phases of Late Pleistocene aggradation and incision in Alaknanda River, western Himalaya, India. *Quaternary Research* 70, 68–80.

Starkel, L., 2003. Climatically controlled terraces in uplifting mountain areas. *Quaternary Science Reviews* 22, 2189–2198.

Suresh, N., Bagati, T.N., Kumar, R., Thakur, V.C., 2007. Evolution of Quaternary alluvial fans and terraces in the intramontane Pinjaur Dun, Sub-Himalaya, NW India: interaction between tectonics and climate change. *Sedimentology* 54, 809–833.

Thakur, V.C., 1983. Palaeotectonic evolution of Indus-Tsangpo Suture Zone in Ladakh and southern Tibet. In: Thakur, V.C., Sharma, K.K. (Eds.), *Geology of Indus Suture Zone of Ladakh*. Wadia Institute of Himalayan Geology, Dehra Dun, India, pp. 195–204.

Thakur, V.C., Misra, D.K., 1984. Tectonic framework of the Indus and Shyok suture zones in the eastern Ladakh, Northwest Himalaya. *Tectonophysics* 101, 207–220.

Thiede, R.C., Bookhagen, B., Arrowsmith, J.R., Sobel, E.R., Strecker, M.R., 2004. Climatic control on rapid exhumation along the Southern Himalayan Front. *Earth and Planetary Science Letters* 222, 791–806.

Thompson, L.G., Yao, T., Davis, M.E., Henderson, K.A., Mosley-Thompson, E., Lin, P.N., Beer, J., Synal, H.A., Cole-Dai, J., Bolzan, J.F., 1997. Tropical climate instability: the last glacial cycle from a Qinghai-Tibetan ice core. *Science* 276, 1821–1825.

Troiani, F., Galve, J.P., Piacentini, D., Seta, M.D., Guerrero, J., 2014. Spatial analysis of stream length-gradient (SL) index for detecting hill slope processes: a case of the Gállego River headwaters (Central Pyrenees, Spain). *Geomorphology* 214, 183–197.

Van Der Beek, P., Melle, J.V., Guillot, S., Pêcher, A., Reiners, P.W., Nicolescu, S., Latif, M., 2009. Eocene Tibetan Plateau remnants preserved in the northwest Himalaya. *Nature Geoscience* 2, 364–368.

Whipple, K.X., Hancock, G.S., Anderson, R.A., 2000. River incision into bedrock: mechanics and relative efficacy of plucking, abrasion, and cavitation. *Geological Society of America Bulletin* 112, 490–503.

Whipple, K.X., Tucker, G.E., 1999. Dynamics of the stream-power river incision model: implications for height limits of mountain ranges, landscape response timescales, and research needs. *Journal of Geophysical Research: Solid Earth* 104, 17661–17674.

Whipple, K.X., Tucker, G.E., 2002. Implications of sediment-flux dependent river incision models for landscape evolution. *Journal of Geophysical Research: Solid Earth* 107, ETG 3-1–ETG 3-20.

Wobus, C., Whipple, K.X., Kirby, E., Snyder, N., Johnson, J., Spyropolou, K., Crosby, B., Sheehan, D., 2006. Tectonics from topography: procedures, promise, and pitfalls. *Geological Society of America, Special Papers* 398, 55–74.

Wu, F.Y., Clift, P.D., Yang, J.H., 2007. Zircon Hf isotopic constraints on the sources of the Indus Molasse, Ladakh Himalaya, India. *Tectonics* 26, TC2014. http://dx.doi.org/10.1029/2006TC002051.

Wünnemann, B., Demske, D., Tarasov, P., Kotlia, B.S., Reinhardt, C., Bloemendal, J., Diekmann, B., *et al*. 2010. Hydrological evolution during the last 15 kyr in the Tso Kar lake basin (Ladakh, India), derived from geomorphological, sedimentological and palynological records. *Quaternary Science Reviews* 29, 1138–1155.